Mon. Not. R. Astron. Soc. **375,** 240–256 (2007) doi:10.1111/j.1365-2966.2006.11286.x

Shock breakout in Type Ibc supernovae and application to GRB 060218/SN 2006aj

Li-Xin Li★
Max-Planck-Institut für Astrophysik, 85741 Garching, Germany

Accepted 2006 November 13. Received 2006 November 2; in original form 2006 May 16

ABSTRACT

Recently, a soft blackbody component was observed in the early X-ray afterglow of GRB 060218, which was interpreted as shock breakout from the thick wind of the progenitor Wolf–Rayet (WR) star of the underlying Type Ic supernova 2006aj. In this paper, we present a simple model for computing the characteristic quantities (including energy, temperature and time duration) for the transient event from the shock breakout in Type Ibc supernovae produced by the core-collapse of WR stars surrounded by dense winds. In contrast to the case of a star without a strong wind, the shock breakout occurs in the wind region rather than inside the star, caused by the large optical depth in the wind. We find that, for the case of a WR star with a dense wind, the total energy of the radiation generated by the supernova shock breakout is larger than that in the case of the same star without a wind by a factor of >10. The temperature can be either hotter or colder, depending on the wind parameters. The time duration is larger caused by the increase in the effective radius of the star due to the presence of a thick wind. Then, we apply the model to GRB 060218/SN 2006aj. We show that, to explain both the temperature and the total energy of the blackbody component observed in GRB 060218 by the shock breakout, the progenitor WR star has to have an unrealistically large core radius (the radius at optical depth of 20), larger than $100\,R_\odot$. In spite of this disappointing result, our model is expected to have important applications to the observations on Type Ibc supernovae in which the detection of shock breakout will provide important clues to the progenitors of Type Ibc supernovae.

Key words: shock waves – supernovae: general – supernovae: individual: SN 2006aj – stars: winds, outflow – stars: Wolf–Rayet – gamma-rays: bursts.

1 INTRODUCTION

Since the first detection of the afterglows (Costa et al. 1997; Frail et al. 1997; van Paradijs et al. 1997) and the host galaxies (Bloom et al. 1998, 1999; Fruchter et al. 1999b) of gamma-ray bursts (GRBs), by now it has well been established that long-duration GRBs are cosmological events occurring in star-forming galaxies (Paczyński 1998a; Fruchter et al. 1999a; Berger, Kulkarni & Frail 2001; Frail et al. 2002; Christensen, Hjorth & Gorosabel 2004; Sollerman et al. 2005; Fruchter et al. 2006 and references therein), and are most likely produced by the core-collapse of massive stars (Woosley, Heger & Weaver 2002; Piran 2004; Zhang & Mészáros 2004; Woosley & Heger 2006a and references therein). This scenario has received strong support from the cumulative evidence that some, if not all, long-duration GRBs are associated with supernovae (SNe), either from direct observations of SN features in the spectra of GRB afterglows, or from indirect observations of rebrightening and/or flattening (called 'red bumps') in GRB afterglows which are interpreted as the emergence of the underlying SN light curves (Della Valle 2006; Woosley & Bloom 2006; Woosley & Heger 2006b and references therein). The discovery of the connection between GRBs and SNe has been one of the most exciting developments in the fields of GRBs and SNe in the past decade.

Interestingly, all the SNe that have been spectroscopically confirmed to be associated with GRBs, including SN 1998bw/GRB 980425 (Galama et al. 1998), SN 2003dh/GRB 030329 (Hjorth et al. 2003b; Stanek et al. 2003), SN 2003lw/GRB 031203 (Malesani et al. 2004; Sazonov, Lutovinov & Sunyaev 2004) and the most recent one, SN 2006aj/GRB 060218 (Campana et al. 2006; Cobb et al. 2006; Masetti et al. 2006; Mirabal et al. 2006; Modjaz et al. 2006; Pian et al. 2006; Sollerman et al. 2006), are Type Ic having no detectable hydrogen and helium lines. However, the SNe that are associated with GRBs also remarkably differ from ordinary Type Ibc SNe: they have extremely smooth and featureless spectra indicating very large expansion velocity, are much more energetic (i.e. involving much larger explosion energy), and eject significantly larger amount of nickels (Hamuy 2004; Della Valle 2006; Woosley

★E-mail: lxl@mpa-garching.mpg.de

& Heger 2006b), except SN 2006aj/GRB 060218 which is somewhat closer to normal Type Ibc SNe (see below; Mazzali et al. 2006). For these reasons, they are often called 'hypernovae' to be distinguished from normal SNe (Iwamoto et al. 1998a; Paczyński 1998a,b). A correlation between the peak spectral energy of GRBs and the peak bolometric luminosity of the underlying SNe is found by Li (2006), based on the multiwavelength observations on the above four pairs of GRBs–SNe.

The discovery of GRB–SN connection has provided us with important clues to the progenitors of GRBs, since it is broadly believed that Type Ibc SNe are produced by the core-collapse of Wolf–Rayet (WR) stars who have lost their hydrogen (possibly also helium) envelopes due to strong stellar winds or interaction with companions (Smartt et al. 2002; Woosley et al. 2002; Filippenko 2004; Woosley & Heger 2006a and references therein). In fact, for several GRBs, observations with high-quality optical spectra have identified the presence of highly ionized lines with high relative velocities most likely coming from shells or clumps of material from WR stars, supporting WR stars as the GRB progenitors (Mirabal et al. 2003; Schaefer et al. 2003; Klose et al. 2004; Chen, Prochaska & Bloom 2006; see, however, Hammer et al. 2006).

A systematic study on the GRB afterglows carried out by Zeh, Klose & Hartmann (2004) suggested that all long-duration GRBs are associated with SNe. However, it appears that only a small fraction of Type Ic SNe are able to produce GRBs, since the rate of GRBs and hypernovae is several orders of magnitude lower than the rate of core-collapse SNe (Podsiadlowski et al. 2004). Although both long-duration GRBs and core-collapse SNe are found in star-forming galaxies, their location in the hosts and the morphology and luminosities of their host galaxies are significantly different as most clearly revealed by the recent study of Fruchter et al. (2006) with *Hubble Space Telescope* (*HST*) imaging. The core-collapse SNe trace the blue light of their hosts that are approximately equally divided between spiral and irregular galaxies, while long GRBs are far more concentrated on the brightest regions of faint and irregular galaxies. Fruchter et al. (2006) argued that their results may be best understood if GRBs are formed from the collapse of extremely massive and low-metallicity stars.

The preference of long-duration GRBs to low-metallicity galaxies (Fynbo et al. 2003; Hjorth et al. 2003a; Le Floc'h et al. 2003; Sollerman et al. 2005; Fruchter et al. 2006) has been strengthened by the recent paper of Stanek et al. (2006), in which a strong anticorrelation between the isotropic energy of five nearby SN-connected GRBs and the oxygen abundance in their host galaxies was found, which was used to argue that the life in the Milky Way is protected away from GRBs by metals. Stanek et al. (2006) have suggested that long-duration GRBs do not trace star formation, but trace the metallicity.

The discovery of GRB 060218 and its association with SN 2006aj by *Swift* has shed more light on the GRB–SN connection as well as on the nature of GRBs. GRB 060218 has a cosmological redshift $z = 0.0335$ corresponding to a luminosity distance of 147 Mpc ($\Omega_{\rm m} = 0.3$, $\Omega_\Lambda = 0.7$ and $H_0 = 70\,{\rm km\,s^{-1}\,Mpc^{-1}}$), which makes it the second nearest GRB among those having determined redshifts (about four times the distance of GRB 980425 at $z = 0.0085$; Campana et al. 2006; Pian et al. 2006; Sollerman et al. 2006). GRB 060218 is very unusual in several aspects. It has an extremely long duration, about 2100 s. Its spectrum is very soft, with a photon index 2.5 ± 0.1 and peak energy $E_{\rm peak} = 4.9^{+0.4}_{-0.3}$ keV in the GRB frame. The isotropic equivalent energy is $E_{\rm iso} = (6.2 \pm 0.3) \times 10^{49}$ erg extrapolated to the 1–10 000 keV in the rest-frame energy band (Campana et al. 2006), which is at least 100 times fainter than normal cosmological GRBs but among a population of underenergetic GRBs (Sazonov et al. 2004; Liang, Zhang & Dai 2006).

Although the SN associated with GRB 060218, i.e. SN 2006aj, is broadly similar to those previously discovered GRB-connected SNe, it also shows some remarkable unusual features (Mazzali et al. 2006; Pian et al. 2006; Sollerman et al. 2006). Among the four GRB-connected SNe mentioned above, SN 2006aj is the faintest one, although still brighter than normal Type Ibc SNe. Its light curve rises more rapidly, and its expansion velocity indicated by the spectrum is intermediate between that of other GRB-connected SNe and that of normal Type Ibc SNe. Modelling of the spectra and the light curve of SN 2006aj reveals that SN 2006aj is much less energetic compared to other GRB-connected SNe: it had an explosion energy $E_{\rm in} \approx 2 \times 10^{51}$ erg, ejected a mass $M_{\rm ej} \approx 2\,{\rm M}_\odot$, compared to $E_{\rm in} \sim 3$–6×10^{52} erg, and $M_{\rm ej} \sim 10\,{\rm M}_\odot$ of the others (Mazzali et al. 2006). This suggests that SN 2006aj is closer to normal Type Ibc SNe than to the other GRB-connected SNe, and there does not exist a clear gap between hypernovae and normal Type Ibc SNe (Li 2006).

The X-ray afterglow observation by the X-Ray Telescope (XRT) on board *Swift* on GRB 060218 started 159 s after the burst trigger. A very interesting feature in the early X-ray afterglow is that it contains a soft blackbody component which has a temperature about 0.17 keV and comprises about 20 per cent of the total X-ray flux in the 0.3–10 keV range, lasting from 159 up to ∼10 000 s. The blackbody component was not detected in later XRT observations (Campana et al. 2006). The total energy contained in the blackbody component, as estimated by Campana (private communication), is $\approx 10^{49}$ erg. Campana et al. (2006) interpreted it as SN shock breakout from a dense wind surrounding the progenitor WR star of the SN.

Butler (2006) conducted an analysis on the early X-ray afterglows of a sample (>70) of GRBs observed by the XRT/*Swift*. He found that although most of the afterglow spectra can be fitted with a pure power law with extinction, a small fraction of them show appreciable soft thermal components at 5–10 per cent level. His reanalysis on GRB 060218 showed that the blackbody component contains energy as much as 2.3×10^{50} erg and has a duration ≈300 s. According to Butler's analysis, the soft blackbody component even dominates the flux after ∼1000 s from the burst trigger.

Flashes from shock breakout in core-collapsed SNe were first predicted by Colgate (1968) almost 40-yr ago, originally proposed for GRBs that had not been discovered yet. However, they have not been unambiguously detected in SN observations yet (Calzavara & Matzner 2004). This is mainly due to the transient nature of the event. It is generally expected that the flash from shock breakout precedes the SN, is much brighter and harder than the SN radiation but has a very short time duration.

According to the general theory of core-collapsed SN explosion, the liberation of explosive energy in the interior of a progenitor star generates a shock wave. The shock wave propagates outwards. However, the external appearance of the star remains unaltered, until the shock wave reaches a point (the shock breakout point) near the stellar surface, where the diffusion velocity of photons begins to exceed the shock velocity. The post-shock radiation can then leak out in a burst of ionizing radiation, producing a brilliant flash in the ultraviolet/X-ray band (Klein & Chevalier 1978; Chevalier & Klein 1979; Imshennik & Nadëzhin 1989; for a comprehensive review, see Matzner & McKee 1999).

For the famous Type II SN 1987A, theoretical calculations have shown that the shock emergence from the surface of the progenitor (Sk 1, a blue supergiant) would have produced a radiation of $\sim 10^{47}$ erg in the extreme ultraviolet to soft X-ray band, lasting 1–3 min (Imshennik & Nadëzhin 1988, 1989; Ensman & Burrows

1992; Blinnikov et al. 2000). In fact, in the observed bolometric light curve of SN 1987A, there was a fast initial decline phase which could be the tail of the light curve produced by the shock breakout (Imshennik & Nadëzhin 1989). If the shock breakout interpretation of the soft blackbody component in GRB 060218 were confirmed, it would have important impact on the theories of both GRBs and SNe. The case of GRB 060218/SN 2006aj would also be the first unambiguous detection of a shock breakout event from SNe.

Although the propagation of a strong shock in a SN and the appearance of shock emergence (shock breakout) have been intensively studied both analytically and numerically (Klein & Chevalier 1978; Imshennik & Nadëzhin 1988, 1989; Ensman & Burrows 1992; Blinnikov et al. 1998; Matzner & McKee 1999; Blinnikov et al. 2000, 2002; Tan, Matzner & McKee 2001), in the situation of SNe produced from stars with dense stellar winds they have not been fully explored yet. If the stellar wind of the progenitor is very optically thick – which is indeed the case for Type Ibc SNe whose progenitors are believed to be WR stars – the shock breakout will occur in the wind region after the shock passes through the surface of the star, instead of in the region inside the star. Since a stellar wind has a mass density profile very different from that of a star, the model that has been developed for the shock emergence in SNe with progenitors without stellar winds cannot be directly applied to the case of progenitors with dense stellar winds.

In this paper, we present a simple model for semi-analytically computing the propagation of a strong shock in a dense stellar wind, and estimating the characteristic quantities for the transient event from the shock breakout in Type Ibc SNe. The model is obtained by an extension of the existing model for the shock propagation and breakout in SNe produced by the core-collapse of stars without dense stellar winds. Then, we apply the model to SN 2006aj and examine if the soft blackbody component in the early X-ray afterglow of GRB 060218 can be interpreted by the SN shock breakout.

The paper is organized as follows. In Section 2, we describe a simple but general model for the mass density and velocity profile for the wind around a WR star, and calculate the optical depth in the wind. In Section 3, we model the propagation of a SN shock wave in a stellar wind, taking into account the relativistic effects. In Section 4, we analyse the evolution of the shock front, and the radiation energy contained in it. In Section 5, we present a procedure for calculating the quantities characterizing the transient event arising from the shock breakout, including the released energy, the temperature, the time duration and the momentum of the shock front at the time of shock breakout. In Section 6, we present our numerical results. In Section 7, we apply our model to GRB 060218/SN 2006aj. In Section 8, we summarize our results and draw our conclusions.

Appendix A is devoted to the formulae for computing the optical depth of a wind in the framework of the standard stellar wind model. Appendix B lists the formulae for computing the characteristic quantities for SN shock breakout from a star without winds, in the trans-relativistic regime. Appendix C presents a correlation among the WR star parameters.

2 MASS DENSITY PROFILE OF THE WIND OF A WR STAR AND THE OPTICAL DEPTH IN THE WIND

WR stars are very luminous, hot and massive stars that are nearly at the end of their stellar lives. Based on their spectra, WR stars are often classified as WN stars (nitrogen dominant) and WC stars (carbon dominant). WR stars are characterized by extremely dense stellar winds, losing mass at a rate of 10^{-6}–$10^{-4}\,\mathrm{M}_\odot\,\mathrm{yr}^{-1}$ with a wind terminal velocity of 700–3000 km s^{-1}. The mass lost from WR stars by stellar winds is so enormous that most (if not all) of hydrogen of WR stars has been lost. This is a main reason for the general belief that WR stars are the progenitors of Type Ibc SNe.

Some basic relations in the physical parameters of WR stars can be found in Langer (1989), Schaerer & Maeder (1992) and Nugis & Lamers (2000).

The wind of a WR star is usually extremely dense. This is characterized by the fact that, for the majority of WR stars, the ratio of the momentum of the wind ($\dot{M}v_\infty$, where $\dot{M}$ is the mass-loss rate and v_∞ is the terminal velocity of the wind) to the momentum of radiation (L/c, where L is the luminosity of the star and c is the speed of light) is much larger than unity, indicating that on average each photon leaving the star must be scattered several times and the wind must be optically thick. As a result, the photospheric radius ($R_{\rm ph}$, the radius where the optical depth $\tau_{\rm w} = 2/3$) often differs from the core radius of the star ($R_\star$, the radius where $\tau_{\rm w} = 20$ by definition) by a factor of >2.

In Fig. 1, we plot the photospheric radius against the core radius for 86 Galactic WC-type and WN-type stars (Hamann, Koesterke & Wessolowski 1995; Koesterke & Hamann 1995) and six Large Magellanic Cloud (LMC) WC-type stars (Gräfener et al. 1998), determined with the 'standard model' of stellar winds. For many WRs, especially those of WC type, we have $R_{\rm ph} > 2R_\star$.

The mass density of a steady and spherically symmetric wind is related to the mass-loss rate and the wind velocity by

$$\rho(r) = \frac{\dot{M}}{4\pi r^2 v_{\rm r}(r)}, \tag{1}$$

where r is the radius from the centre of the star and $v_{\rm r}$ is the radial velocity of the wind. We model the velocity of the wind by (Schaerer 1996; Ignace, Oskinova & Foullon 2000; Nugis & Lamers 2002)

$$v_{\rm r}(r) = v_\infty \left(1 - \frac{\alpha R_\star}{r}\right)^b, \tag{2}$$

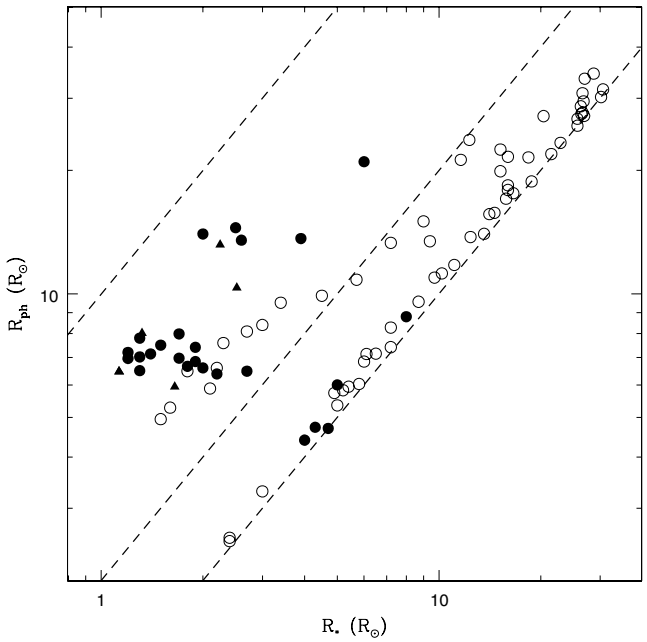

Figure 1. Photospheric radius versus stellar core radius, for 86 Galactic WRs (filled circles for WC type and open circles for WN type) and six LMC WRs (triangles, WC type only). The dashed lines show the relation of $R_{\rm ph} = R_\star$, $R_{\rm ph} = 2R_\star$ and $R_{\rm ph} = 10R_\star$ (upward).

where $\alpha < 1$ and $b \geqslant 1$ are free parameters. The presence of α in equation (2) is to ensure that the mass density of the wind is regular at the stellar radius $r = R_\star$.

In the 'standard model' of stellar winds, the value of b is assumed to be unity, as in the case of O-stars. However, it has been argued that for WR stars b can be significantly larger (Robert 1994; Schmutz 1997; Lépine & Moffat 1999). According to the calculations of Nugis & Lamers (2002), b is typically in the range of 4–6.

The value of α can be determined by the radial velocity of the wind at $r = R_\star$. If we define $\varepsilon = v_\star/v_\infty$, where $v_\star \equiv v_{\rm r}(R_\star)$, then

$$\alpha = 1 - \varepsilon^{1/b}. \tag{3}$$

Typically, $v_\star$ has the order of the sound speed at $R_\star$, and $\varepsilon \sim 0.01$ (Schaerer 1996).

In the outer wind region, where $r \gg R_\star$ and $v_{\rm r} \approx v_\infty$, the wind density $\rho \sim r^{-2}$. In the region close to the stellar surface (i.e. $r \sim R_\star$), the wind density has a much steeper log slope (Fig. 2). As will be seen in Section 3, it is the very steep mass density profile near the surface of the star that makes it possible for a shock wave to accelerate in the wind region. We will also see in Section 6 that shock breakout takes place at a radius not far from the surface of $r = R_\star$. Therefore, we adopt equation (2) for the wind velocity profile since its asymptotic form $v_{\rm r} = v_\infty$ (and $\rho \propto r^{-2}$) is not accurate for describing the wind velocity (and hence the mass density) near $r = R_\star$.

The opacity $\kappa_{\rm w}$ in the WR wind region is complex and generally a function of radius (Nugis & Lamers 2002; Gräfener & Hamman 2005). However, compared to the mass density, the opacity changes very slowly with radius. For example, at the sonic point in the wind, we have $|{\rm d}\ln\kappa_{\rm w}/{\rm d}\ln r| \sim 0.001$–$0.03$ (Nugis & Lamers 2002), while $|{\rm d}\ln\rho/{\rm d}\ln r| \gtrsim 2$ always. Hence, to calculate the optical depth in the wind, we can approximate $\kappa_{\rm w}$ by a constant although its value is uncertain at some level. Then, the optical depth in the wind is

$$\tau_{\rm w} \equiv \int_r^\infty \kappa_{\rm w}\rho {\rm d}r = \frac{A}{(b-1)\alpha R_\star}\left[\left(1-\frac{\alpha}{y}\right)^{1-b} - 1\right], \tag{4}$$

where $y \equiv r/R_\star$ and $A \equiv \kappa_{\rm w}\dot{M}/(4\pi v_\infty)$.

As commonly adopted in the literature, we define the stellar core radius $R_\star$ of the WR star to be the radius where $\tau_{\rm w} = 20$. Then, we can rewrite the optical depth as

$$\tau_{\rm w} = \tau_0\left[\left(1-\frac{\alpha}{y}\right)^{1-b} - 1\right], \tag{5}$$

where

$$\tau_0 \equiv \frac{A}{(b-1)\alpha R_\star} = \frac{20}{(1-\alpha)^{1-b}-1}. \tag{6}$$

By definition, the boundary of the photosphere is at the photospheric radius where $\tau_{\rm w} = 2/3$. Then, we can solve for $y_{\rm ph} \equiv R_{\rm ph}/R_\star$ from equation (5)

$$y_{\rm ph} = \alpha\left[1-\left(1+\frac{2}{3\tau_0}\right)^{1/(1-b)}\right]^{-1}. \tag{7}$$

For a given b, $y_{\rm ph}$ is a decreasing function of α. As $\alpha \to 1$, we have $\tau_0 \to 0$ and $y_{\rm ph} \to 1$. As $\alpha \to 0$, we have $\tau_0 \approx 20/[(b-1)\alpha]$ and $y_{\rm ph} \to 30$. Thus, in general we must have $1 < y_{\rm ph} < 30$. By equation (3), α is a decreasing function of ε.

The above results for the optical depth are valid only for $b > 1$. The corresponding formulae for $b = 1$ (the 'standard model') are given in Appendix A.

In Fig. 3, we plot α versus $y_{\rm ph}$, solved from equations (3) and (7) (or equation A3 when $b = 1$) for a set of discrete values of b (from 1 to 10) and continuous values of ε (from 10^{-5} to 10^{-1}). The value of $y_{\rm ph}$ sensitively depends on ε. For the same value of b, $y_{\rm ph}$ drops quickly as ε decreases. When ε is fixed, $y_{\rm ph}$ decreases if b increases

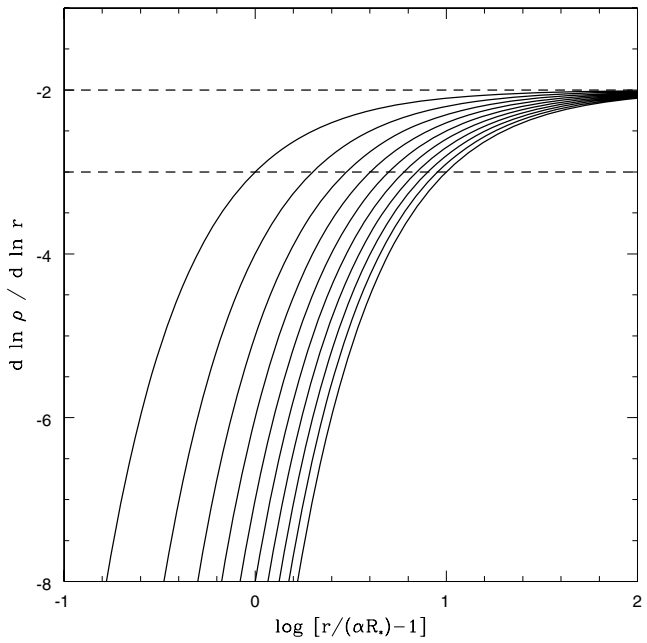

Figure 2. The log slope of the wind density, $s \equiv {\rm d}\ln\rho/{\rm d}\ln r = -2 - b(r/\alpha R_\star - 1)^{-1}$, as a function of the radius r. As $r \to \infty$, s approaches -2 (the upper dashed line). For small r, s is significantly smaller than -2. A shock wave accelerates only in the region of $s < -3$ (below the lower dashed line; see Section 3). Left to right: $b = 1$–10 with $\Delta b = 1$.

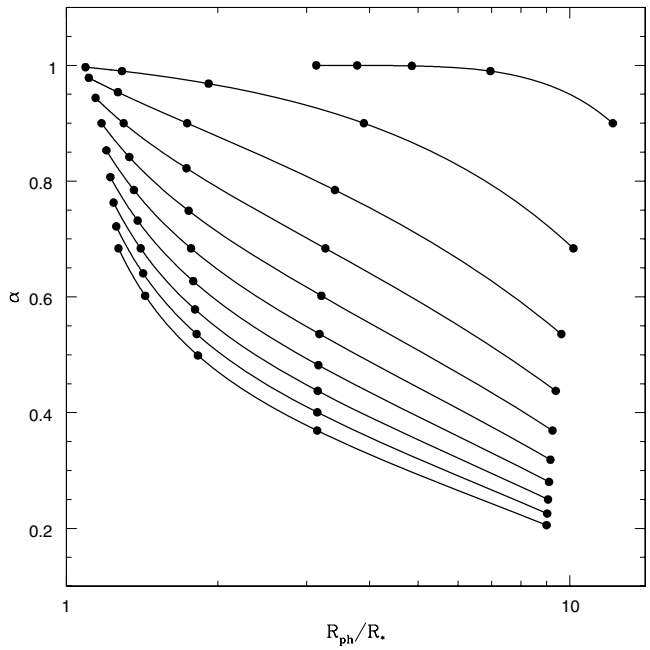

Figure 3. The solution for α and $y_{\rm ph} = R_{\rm ph}/R_\star$, for $\varepsilon = 10^{-5}$–10^{-1}. Top to bottom: $b = 1$–10 with $\Delta b = 1$. The filled circles on each curve label the values of $\varepsilon = 10^{-5}$, 10^{-4}, 10^{-3}, 10^{-2} and 10^{-1} from left to right.

from $b = 1$, very fast for small values of ε. However, for $b > 3$, the effect of the variation in b on the value of $y_{\rm ph}$ is not dramatic.

The opacity $\kappa_{\rm w}$, and the corresponding optical depth $\tau_{\rm w}$, are for the optical photons in the wind and are hence valid for calculating the mass density profile of the wind before a SN shock passes through it. As will be seen in the following sections, the radiation generated by the SN shock wave in the wind of a WR star is in the X-ray band and we also need to consider the opacity and the optical depth to the X-ray photons for computing the thickness of the shock front and the emergence of the shock wave (Sections 4 and 5).

The X-ray opacity of a gas strongly depends on the ionization state of the gas (Krolik & Kallman 1984). The radiation generated by a SN shock wave in the wind of a WR star has a luminosity $L_{\rm X} \gtrsim 10^{45}$ erg s^{-1} (Sections 5 and 6), which contains enough photons to fully ionize the surrounding gas. This fact can be seen from the ionization parameter, defined as the ratio of the photon number density to the particle number density, $\Xi \equiv L_{\rm X}/(4\pi c r^2 n_{\rm H} \varepsilon_{\rm ph})$, where $\varepsilon_{\rm ph}$ is the energy of photons. Using equation (1) (where $v_{\rm r} \approx v_\infty$) and $n_{\rm H} = \rho/\mu_{\rm H} m_{\rm H}$, where $m_{\rm H}$ is the mass of proton and $\mu_{\rm H} \approx 2$ is the mean molecular weight per proton, we get

$$\Xi \approx \frac{\mu_{\rm H} m_{\rm H} L_{\rm X} v_\infty}{\dot{M} \varepsilon_{\rm ph} c} \approx 4.4 \times 10^6 \, \mu^{-1} \left(\frac{L_{\rm X}}{10^{45} \, {\rm erg \, s^{-1}}} \right) \left(\frac{\varepsilon_{\rm ph}}{1 \, {\rm keV}} \right)^{-1}, \quad (8)$$

where

$$\mu \equiv \left(\frac{\dot{M}}{5 \times 10^{-5} \, {\rm M_\odot \, yr^{-1}}} \right) \left(\frac{v_\infty}{2000 \, {\rm km \, s^{-1}}} \right)^{-1}. \quad (9)$$

Hence, for typical parameters we have $\Xi \gtrsim 10^6$, which means that a tiny fraction of the radiation would be enough to fully ionize the gas in the wind. Then, the absorption opacity is negligible (Krolik & Kallman 1984). The opacity in the wind to the X-ray photons is then dominated by the electron-scattering opacity, $\kappa_{\rm es} = 0.2 \, {\rm cm^2 \, g^{-1}}$, which is insensitive to the photon energy if the photon energy is much smaller than the electron mass energy (Akhiezer & Berestetskii 1965).

The X-ray optical depth in the wind is

$$\tau_{\rm X} \equiv \kappa_{\rm es} \int_r^\infty \rho \, {\rm d}r = \iota \tau_{\rm w}, \qquad \iota \equiv \frac{\kappa_{\rm es}}{\kappa_{\rm w}}. \quad (10)$$

The X-ray photospheric radius, defined by $\tau_{\rm X} = 2/3$, is then

$$y_{\rm ph,X} = \alpha \left[1 - \left(1 + \frac{2}{3\iota\tau_0} \right)^{1/(1-b)} \right]^{-1}. \quad (11)$$

3 PROPAGATION OF A STRONG SHOCK WAVE IN THE WIND

The propagation of a strong shock wave in a gas is determined by two competing processes: the collection of mass from the ambient gas makes the shock wave decelerate, and the steep downward gradient of the gas mass density makes the shock wave accelerate. Based on previous self-similar analytical solutions and numerical works, Matzner & McKee (1999) have proposed a continuous and simple form for the shock velocity that accommodates both spherical deceleration and planar acceleration

$$v_{\rm s} \propto \left(\frac{E_{\rm in}}{m} \right)^{1/2} \left(\frac{\rho r^3}{m} \right)^{-\beta_1}, \quad (12)$$

where $\beta_1 \approx 0.2$. In the above equation, $E_{\rm in}$ is the explosion kinetic energy, $m(r) \equiv M(r) - M_{\rm rem}$, $M_{\rm rem}$ is the mass of the material that will become the SN remnant and $M(r)$ is the mass of the material contained in radius r.

After the shock has collected an enough amount of mass so that $m(r)$ does not change significantly any more, we have $v_{\rm s} \propto (\rho r^3)^{-\beta_1}$, the behaviour of the shock is purely determined by the profile of the mass density in the region that the shock is plowing into. Then, for a spherically symmetric gas, the shock wave accelerates when ${\rm d}(\rho r^3)/{\rm d}r < 0$ and decelerates when ${\rm d}(\rho r^3)/{\rm d}r > 0$.

To generalize the formalism to the case of a relativistic shock wave, Gnatyk (1985) has suggested to replace the shock velocity $v_{\rm s}$ on the left-hand side of equation (12) by $\Gamma_{\rm s}\beta_{\rm s}$, where $\beta_{\rm s} \equiv v_{\rm s}/c$, c is the speed of light, and $\Gamma_{\rm s} \equiv (1 - \beta_{\rm s}^2)^{-1/2}$ is the Lorentz factor. The equation so obtained quite accurately describes both the limits of non-relativistic ($\beta_{\rm s}^2 \ll 1$, i.e. $\Gamma_{\rm s} \approx 1$) and ultrarelativistic ($\beta_{\rm s}^2 \approx 1$, i.e. $\Gamma_{\rm s} \gg 1$) shocks. However, Tan et al. (2001) have shown that it is not accurate in the trans-relativistic regime ($\beta_{\rm s}^2$ is close to 1 but $\Gamma_{\rm s}$ is not large enough). Tan et al. (2001) have suggested the following formula for both non-relativistic and trans-relativistic shocks

$$\Gamma_{\rm s}\beta_{\rm s} = p(1 + p^2)^{0.12},$$
$$p \equiv 0.736 \left(\frac{E_{\rm in}}{mc^2} \right)^{1/2} \left(\frac{\rho r^3}{m} \right)^{-0.187}. \quad (13)$$

With numerical simulation, Tan et al. (2001) have verified equation (13) for trans-relativistic and accelerating shocks with $\Gamma_{\rm s}\beta_{\rm s}$ up to a value $\sim$10. However, the limited numerical resolution in their code has not allowed them to follow the acceleration of a non-relativistic shock into the ultrarelativistic regime (Tan et al. 2001).

Although equation (13) has never been tested on relativistic and decelerating shock waves, in the non-relativistic limit it returns to the formula of Matzner & McKee, i.e. equation (12), which applies to both accelerating and decelerating shocks. Hence, we assume that equation (13) applies to both accelerating and decelerating relativistic shocks.

Because of the compactness of WR stars, the problem that we are solving here is right in the trans-relativistic regime (as will be confirmed latter in this paper). Thus we will use equation (13) to calculate the momentum of a shock wave propagating in a wind of a WR star. In addition, since the wind contains a negligible amount of mass, at the radius where shock breakout takes place (either inside the star but close to its surface, or in the wind region), we have $m \approx M_{\rm ej}$, where $M_{\rm ej}$ is the ejected mass.

Although the equation for the shock movement that we use in this paper is the same as that used by Matzner & McKee (1999) and Tan et al. (2001), the mass density profile in the wind of a star is very different from that in the interior of a star. In the outer layer of a star, the mass density drops quickly as the radius increases by a very small amount, as described by equation (B1). Hence, as the shock wave approaches the surface of the star, it always accelerates according to $v_{\rm s} \propto \rho^{-\beta_1}$ since $m \approx M_{\rm ej}$ and $r \approx R_\star$.

The situation is very different in a stellar wind. A shock wave propagating in a wind with a density given by equations (1) and (2) accelerates in the region near the stellar surface $r = R_\star$, but decelerates at large radius since $\rho \propto r^{-2}$ and ${\rm d}(\rho r^3)/{\rm d}r > 0$ for $r \gg R_\star$ (Fig. 2). The transition from acceleration to deceleration occurs at a radius determined by ${\rm d}(\rho r^3)/{\rm d}r = 0$, where the shock velocity reaches the maximum. The transition radius is found to be

$$R_{\rm a} = (1 + b)\alpha R_\star. \quad (14)$$

After passing the transition radius, the shock wave starts decelerating. The maximum $\Gamma_{\rm s}\beta_{\rm s}$ is then obtained by substituting $r = R_{\rm a}$

in equation (13)

$$(\Gamma_s\beta_s)_{\max} = p_{\max}\left(1+p_{\max}^2\right)^{0.12},$$
$$p_{\max} = 1.181\,[\alpha f(b)]^{-0.187} \times \left(\frac{E_{\rm in}}{M_{\rm ej}c^2}\right)^{1/2}\left(\frac{\Psi}{M_{\rm ej}}\right)^{-0.187}, \quad (15)$$

where $f(b) \equiv (1+b)(1+1/b)^b$, and the mass function Ψ is defined by

$$\Psi \equiv \frac{\dot{M}R_\star}{v_\infty} = 1.654\times10^{-9}\,{\rm M}_\odot\,\mu\left(\frac{R_\star}{3\,{\rm R}_\odot}\right), \quad (16)$$

where μ is defined by equation (9).

The function Ψ is an estimate of the mass contained in the photosphere region of the wind. A correlation between Ψ and $R_{\rm ph}$ is presented in Appendix C.

Submitting typical numbers into equations (15) and (16), we get

$$p_{\max} = 1.137\mu^{-0.187}\left[\frac{\alpha f(b)}{f(5)}\right]^{-0.187}\left(\frac{E_{\rm in}}{10^{52}\,{\rm erg}}\right)^{0.5} \times \left(\frac{M_{\rm ej}}{10\,{\rm M}_\odot}\right)^{-0.313}\left(\frac{R_\star}{3\,{\rm R}_\odot}\right)^{-0.187}. \quad (17)$$

Thus, typically, the shock wave is trans-relativistic.

4 ENERGY OF THE RADIATION CONTAINED IN THE SHOCK FRONT

The gas pressure behind a relativistic shock front, measured in the frame of the shocked gas, is (Blandford & McKee 1976)

$$p_2 = (\gamma_2-1)(\hat{\gamma}_2\gamma_2+1)\rho c^2, \quad (18)$$

where $\hat{\gamma}_2$ is the polytropic index of the shocked gas, γ_2 is the Lorentz factor of the shocked gas and ρ is the mass density of the unshocked gas. The Lorentz factor γ_2 is related to the Lorentz factor of the shock front $\Gamma = \Gamma_s$ by equation (5) of Blandford & McKee (1976). Since WR winds are radiation dominated, we have $\hat{\gamma}_2 = 4/3$. Then, we can approximate p_2 by

$$p_2 \approx F_p(\Gamma_s\beta_s)\,\rho\Gamma_s^2 v_s^2, \quad (19)$$

where $F_p(\Gamma_s\beta_s) \sim 1$ is defined by

$$F_p(x) \equiv \frac{2}{3} + \frac{4}{21\left(1+0.4252\,x^2\right)^{0.4144}}, \quad (20)$$

which has the correct asymptotic values as $\Gamma_s\beta_s \to \infty$ (ultrarelativistic limit) and $\Gamma_s\beta_s \to 0$ (non-relativistic limit), and has a fractional error <0.3 per cent in the trans-relativistic regime.

Denoting the temperature of the radiation behind the shock front by T_2, then the pressure of the radiation measured in the frame of the shocked gas is

$$\frac{1}{3}aT_2^4 \approx p_2 \approx F_p(\Gamma_s\beta_s)\,\rho\Gamma_s^2 v_s^2, \quad (21)$$

where a is the radiation density constant.

A strong shock has a very narrow front. In the non-relativistic limit, the geometric thickness of the shock front is (Imshennik & Nadëzhin 1988, 1989)

$$\Delta r_s \approx \frac{c}{\kappa_{\rm es}\rho v_s}, \quad (22)$$

where $\kappa_{\rm es}$ is the electron-scattering opacity (see Section 2). That is, the thickness of the shock front is equal to the mean free path of photons multiplied by the optical depth of the shock

$$\tau_s = \frac{c}{v_s}. \quad (23)$$

For an ultrarelativistic blast wave, the total energy stored in the shock wave is proportional to $\Gamma_s^2 r^3$ and hence the thickness of the shell of shocked particles is $\sim r/\Gamma_s^2$ (Blandford & McKee 1976). That is, in the ultrarelativistic limit, the thickness of the shock front measured in the rest frame is $\propto \Gamma_s^{-2}$. Hence, using the optical depth of the shock and that of the wind, we can estimate the geometric thickness of a relativistic shock front in the rest frame by

$$\Delta r_s \approx \xi\frac{\tau_s}{\tau_X}\frac{r}{\Gamma_s^2}, \quad (24)$$

where τ_X is the X-ray optical depth (equation 10) and

$$\xi \equiv \frac{\tau_X}{\kappa_{\rm es}\rho r} = \left|\frac{\partial\ln\tau_X}{\partial\ln r}\right|^{-1} = \frac{y}{\alpha(b-1)}\left[1-\frac{\alpha}{y}-\left(1-\frac{\alpha}{y}\right)^b\right]. \quad (25)$$

Equation (24) returns to equation (22) in the non-relativistic limit. The function $\xi(y)$ is an increasing function of y. As $y \to \infty$, we have $\xi \to 1$. As $y \to \alpha$, we have $\xi \to 0$. (When $b = 1$, ξ is given by equation A6 in Appendix A.)

The total energy of the radiation contained in the shock front, measured in the frame of the shocked gas, is then

$$E_{\rm R} \approx \frac{1}{3}\left(aT_2^4\right)4\pi r^2(\gamma_2\Delta r_s) \approx \frac{4\pi\tau_s\gamma_2}{3\tau_X\Gamma_s^2}\xi\left(aT_2^4\right)r^3, \quad (26)$$

where the factor 1/3 accounts for the fact that the energy density is not uniform (concentrated at the boundary of the shock) and the factor γ_2 in $(\gamma_2\Delta r_s)$ accounts for the Lorentz contraction. Substituting equation (21) in equation (26), we get

$$E_{\rm R} \approx \frac{4\pi\tau_s\gamma_2}{\tau_X\Gamma_s^2}\xi F_p(\Gamma_s\beta_s)\,\rho r^3\Gamma_s^2 v_s^2. \quad (27)$$

Using the definition of ξ, we have

$$E_{\rm R} \sim \frac{4\pi\gamma_2 c}{\Gamma_s^2\kappa_{\rm es}v_s}F_p r^2\Gamma_s^2 v_s^2 \propto r^2\Gamma_s v_s,$$

since $F_p \sim 1$ and $\gamma_2/\Gamma_s \sim 1$.

In the accelerating region ($r < R_a$), $\Gamma_s v_s$ and γ_2 increase with r. Hence, the total energy contained in the shock front as measured by the rest observer, $\gamma_2 E_{\rm R}$, increases with r.

In the decelerating region ($r > R_a$, $\rho \sim r^{-2}$), by equation (13) we have, approximately, $\Gamma_s v_s \propto r^{-0.2}$, thus $E_{\rm R} \propto r^{1.8}$. In the non-relativistic limit, $\gamma_2 E_{\rm R} \approx E_{\rm R} \propto r^{1.8}$. In the ultrarelativistic limit, $\gamma_2 E_{\rm R} \propto \gamma_2 r^{1.8} \propto r^{1.6}$ since $\gamma_s = \Gamma_s/\sqrt{2} \propto r^{-0.2}$. Hence, in the region of $r > R_a$, we also expect that the total energy contained in the shock front, $\gamma_2 E_{\rm R}$, increases with r although the shock is decelerating. This is caused by the fact that the volume contained in the shock front increases with r.

5 EMERGENCE OF THE SHOCK AND THE CHARACTERISTIC QUANTITIES

Inside the star or deep inside the wind, because of the large optical depth in the gas photons has a diffusion velocity that is smaller than the velocity of the shock front, so that the radiation generated by the shock wave is trapped inside the boundary of the shock. As the

shock wave moves towards the boundary of the photosphere, the optical depth in the gas drops, until a radius is reached where the diffusion velocity of photons begins to exceed the velocity of the shock front. Then, the radiation generated by the shock wave starts to escape from the star to produce a bright flash, and the shock becomes visible to a remote observer.

Thus, the shock emerges at a radius where the optical depth of the gas to the radiation generated by the shock is equal to the optical depth of the shock

$$\tau_{\rm X} = \frac{c}{v_{\rm s}}, \tag{28}$$

since beyond that radius photons diffuse outwards faster than the shock front moves (Imshennik & Nadëzhin 1988, 1989; Matzner & McKee 1999). Since $v_{\rm s} < c$ always, the shock must emerge at a radius where $\tau_{\rm X} > 1$. By equations (5) and (10), the maximum breakout radius (determined by $\tau_{\rm X} = 1$) is at

$$y_{\rm max} = \alpha \left[1 - \left(1 + \frac{1}{\iota \tau_0} \right)^{1/(1-b)} \right]^{-1}, \tag{29}$$

which is approached by an ultrarelativistic shock. [When $b = 1$, $y_{\rm max}$ is given by equation (A7).]

The evolution of $\Gamma_{\rm s}\beta_{\rm s}$ is determined by equation (13), which can be recast into

$$\Gamma_{\rm s}\beta_{\rm s} = p(1+p^2)^{0.12},$$
$$p = 1.181 \left(\frac{E_{\rm in}}{M_{\rm ej}c^2} \right)^{1/2} \left(\frac{\Psi}{M_{\rm ej}} \right)^{-0.187} \times y^{-0.187} \left(1 - \frac{\alpha}{y} \right)^{-0.187b}, \tag{30}$$

where equations (1) and (2) have been used, and Ψ is the mass function defined by equation (16).

With equations (30), (10) and (5) (or A1 if $b = 1$), we can calculate the radius where the shock breakout takes place, $R_{\rm br} \equiv y_{\rm br} R_\star$, by numerically solving the algebraic equation (28).

After having $y_{\rm br}$, we can calculate the momentum of the shock wave at $y = y_{\rm br}$, by equation (30).

Since the shock breakout occurs at a radius, where $\tau_{\rm s} = \tau_{\rm X}$ (equation 28), by equation (27), the total energy of the radiation generated by the shock breakout as measured by a rest observer is

$$E_{\rm br} \equiv [\gamma_2 E_{\rm R}]_{r=R_{\rm br}} \approx 4\pi\xi F_\gamma^2 F_p \, \rho r^3 \Gamma_{\rm s}^2 v_{\rm s}^2 \big|_{r=R_{\rm br}}, \tag{31}$$

where $F_p = F_p(\Gamma_{\rm s}\beta_{\rm s}) \sim 1$, $F_\gamma = F_\gamma(\Gamma_{\rm s}) \equiv \gamma_2/\Gamma_{\rm s} \sim 1$. The Lorentz factors γ_2 and $\Gamma_{\rm s}$ are related by the equation (5) of Blandford & McKee (1976). For the case of $\hat{\gamma}_2 = 4/3$, F_γ can be approximated by

$$F_\gamma(x) \approx \frac{1}{\sqrt{2}} + \frac{1 - 1/\sqrt{2}}{[1 + 0.9572\,(x-1)]^{0.9325}},$$

which gives the correct asymptotic values at the non-relativistic limit ($\Gamma_{\rm s} \to 1$) and the ultrarelativistic limit ($\Gamma_{\rm s} \to \infty$), and has a fractional error <0.08 per cent in the trans-relativistic case.

Substituting equations (1) and (2) in equation (31) and using equation (16), we get

$$E_{\rm br} \approx \Psi c^2 \left[\xi F_\gamma^2 F_p \Gamma_{\rm s}^2 \beta_{\rm s}^2 \right]_{y=y_{\rm br}} y_{\rm br} \left(1 - \frac{\alpha}{y_{\rm br}} \right)^{-b}$$
$$\approx 1.48 \times 10^{46}\,{\rm erg}\, \mu \left(\frac{R_\star}{3\,{\rm R}_\odot} \right) \left(\frac{y_{\rm br}}{5} \right) \left(1 - \frac{\alpha}{y_{\rm br}} \right)^{-b} \times \left[\xi F_\gamma^2 F_p \Gamma_{\rm s}^2 \beta_{\rm s}^2 \right]_{y=y_{\rm br}}. \tag{32}$$

Similarly, from equation (21), we can obtain the temperature of the radiation measured in a rest frame

$$T_{\rm br} \equiv [\gamma_2 T_2]_{r=R_{\rm br}}$$
$$\approx \left(\frac{3\Psi c^2}{4\pi a R_\star^3} \right)^{1/4} \left[F_\gamma F_p^{1/4} \Gamma_{\rm s}^{3/2} \beta_{\rm s}^{1/2} \right]_{y=y_{\rm br}} \times y_{\rm br}^{-1/2} \left(1 - \frac{\alpha}{y_{\rm br}} \right)^{-b/4}$$
$$\approx 0.800 \times 10^6\,{\rm K}\, \mu^{0.25} \left(\frac{R_\star}{3\,{\rm R}_\odot} \right)^{-0.5} \left(\frac{y_{\rm br}}{5} \right)^{-0.5} \times \left(1 - \frac{\alpha}{y_{\rm br}} \right)^{-b/4} \left[F_\gamma F_p^{1/4} \Gamma_{\rm s}^{3/2} \beta_{\rm s}^{1/2} \right]_{y=y_{\rm br}}. \tag{33}$$

The time duration of the shock breakout event is set by the time spent by a photon to diffuse out to the surface of the photosphere from the breakout radius. Since at the radius of shock breakout the diffusion velocity of photons is equal to the velocity of the shock wave, we have

$$t_{\rm br} \approx \frac{R_{\rm ph,X} - R_{\rm br}}{v_{\rm s,br}} = \frac{R_\star}{\beta_{\rm s,br} c} (y_{\rm ph,X} - y_{\rm br})$$
$$\approx 6.96\,{\rm s} \left(\frac{R_\star}{3\,{\rm R}_\odot} \right) \beta_{\rm s,br}^{-1} (y_{\rm ph,X} - y_{\rm br}), \tag{34}$$

where $R_{\rm ph,X} = y_{\rm ph,X} R_\star$ is the X-ray photospheric radius (equations 11 and A4), and $v_{\rm s,br} = \beta_{\rm s,br}\, c \equiv v_{\rm s}(r = R_{\rm br})$ is the speed of the shock wave at the time of breakout.

6 RESULTS

Unlike in the cases of non-relativistic and ultrarelativistic shock waves, where the quantities characterizing the transient event from the shock breakout can be expressed with factorized scaling relations of input parameters (e.g. equations 36–38 of Matzner & McKee 1999), in the trans-relativistic case here we must numerically solve the relevant equations for the characteristic quantities.

All the relevant equations are in Section 5, supplemented by the formulae for the wind mass function Ψ and the optical depth in Sections 2 and 3 (and Appendix A when $b = 1$). We can eliminate $\dot{M}$ and v_∞ from the equations by using

$$\Psi = \frac{80\pi(b-1)\alpha R_\star^2}{\kappa_{\rm w}[(1-\alpha)^{1-b} - 1]}, \tag{35}$$

which is obtained by substituting equation (6) in the definition of Ψ (equation 16). [When $b = 1$, the corresponding equation is (A5).] Since α is a function of ε and b (equation 3), we can then choose the input parameters to be $E_{\rm in}$, $M_{\rm ej}$, $R_\star$, ε, b and $\kappa_{\rm w}$.

Note, two opacities are involved in our model $\kappa_{\rm w}$, the optical opacity in the wind of a WR star, which is used to calculate the mass density profile in the wind before the shock wave passes through it; $\kappa_{\rm X} = \kappa_{\rm es}$, the X-ray opacity in the wind, which is used to calculate the interaction of the X-ray photons generated by the shock wave with particles in the wind (see Section 2). Since $\kappa_{\rm es} = 0.2\,{\rm cm^2\,g^{-1}}$ is a constant but $\kappa_{\rm w}$ is somewhat uncertain, we treat $\kappa_{\rm w}$ as an input parameter.

Compared to the case of shock breakout from a star without a wind (Matzner & McKee 1999, and Appendix B in this paper), here we have two additional parameters, ε and b, both describing the shape of the wind velocity profile (equations 2 and 3). However, in the case of a star, the opacity is fairly well determined so there are essentially only three parameters: the explosion energy $E_{\rm in}$, the

ejected mass $M_{\rm ej}$ and the stellar radius $R_\star$. Although there is yet another parameter $\zeta \equiv \rho_1/\rho_\star$ (see Appendix B), which is typically 0.2 for blue supergiants and 0.5 for red supergiants (Calzavara & Matzner 2004), the characteristic quantities (at least the energy, the temperature and the shock momentum) at shock breakout are very insensitive to ζ (Matzner & McKee 1999). While for the problem here, i.e. a dense stellar wind surrounding a star, the opacity $\kappa_{\rm w}$ is poorly known. Modelling of the WR winds indicates that $\kappa_{\rm w}$ is in the range of 0.3–0.9 cm^2 g^{-1} at the sonic point, and slightly larger at larger radii (Nugis & Lamers 2002).

The parameter ε, which is the ratio of the wind velocity at the stellar surface to the terminal velocity of the wind, is usually thought to be in the range of 0.001–0.1, and typically around 0.01 (Schaerer 1996).

The parameter b, which characterizes the log slope of the wind velocity in the region near the stellar surface, is taken to be unity in the 'standard model' of stellar winds. However, as already mentioned in Section 2, for the winds of WR stars b can be much larger than unity as argued by Robert (1994), Schmutz (1997) and Lépine & Moffat (1999), and is typically in the range of 4–6 (Nugis & Lamers 2002).

In our numerical modelling, we allow $\kappa_{\rm w}$ to vary from 0.2 to 0.9 cm^2 g^{-1}, ε to vary from 10^{-5} to 10^{-1} and b from 1 to 10. We allow $E_{\rm in}$ to vary from 10^{51} (for normal core-collapse SNe) to 10^{53} erg (for hypernovae), $M_{\rm ej}$ to vary from 1 to 20 $\rm M_\odot$. Although WR stars are compact and have small radii, to fully explore the effect of variation in the stellar radius on the results, we allow $R_\star$ to vary from 1 to 30 $\rm R_\odot$. Whenever numbers are quoted, we refer to the fiducial values $\kappa_{\rm w} = 0.7$ cm^2 g^{-1}, $\varepsilon = 0.01$, $b = 5$, $E_{\rm in} = 10^{52}$ erg, $M_{\rm ej} = 10\,\rm M_\odot$ and $R_\star = 3\,\rm R_\odot$, unless otherwise stated.

Our numerical results for the characteristic quantities of the shock breakout, including the total energy ($E_{\rm br}$; equation 32), the temperature ($T_{\rm br}$; equation 33), the time duration ($t_{\rm br}$; equation 34) and the shock momentum ($\Gamma_{\rm s,br}\,\beta_{\rm s,br}$; equation 30 with $y = y_{\rm br}$) are presented in Figs 4–8.

Fig. 4 shows $E_{\rm br}$, $T_{\rm br}$, $t_{\rm br}$ and $\Gamma_{\rm s,br}\,\beta_{\rm s,br}$ as functions of the opacity $\kappa_{\rm w}$. Solid lines correspond to $\varepsilon = 10^{-2}$. Dashed lines correspond to $\varepsilon = 10^{-3}$. Other parameters take the fiducial values, as indicated in the figure caption. For $\varepsilon = 10^{-2}$, $E_{\rm br}$ is a slow but not monotonic function of $\kappa_{\rm w}$. For $\varepsilon = 10^{-3}$, $E_{\rm br}$ increases with $\kappa_{\rm w}$. As $\kappa_{\rm w}$ increases from 0.2 to 0.9 cm^2 g^{-1}, $E_{\rm br}$ increases by a factor of $\approx$1.2 when $\varepsilon = 10^{-2}$ and $\approx$2.6 when $\varepsilon = 10^{-3}$. The temperature $T_{\rm br}$ increases by a factor of $\approx$4 in both cases. The opacity $\kappa_{\rm w}$ has also an effect on $t_{\rm br}$, which decreases by a factor of $\approx$4 when $\varepsilon = 10^{-2}$, and $\approx$2.6 when $\varepsilon = 10^{-3}$. Similar to the temperature, the momentum of the shock front is also an increasing function of $\kappa_{\rm w}$. As $\kappa_{\rm w}$ increases from 0.2 to 0.9 cm^2 g^{-1}, $\Gamma_{\rm s,br}\beta_{\rm s,br}$ increases by a factor of $\approx$2.2 (for both $\varepsilon = 10^{-2}$ and 10^{-3}). Similar to the case of breakout from a star, the results do not change dramatically with the opacity if b is around 5. Thus, the poor knowledge in the opacity in the stellar winds will not affect our results drastically.

All the dependence on $\kappa_{\rm w}$ manifests itself though the mass function Ψ in equation (35) (and equation A5 when $b = 1$), which shows that $\Psi \propto \kappa_{\rm w}^{-1}$. Then, from the condition for the shock breakout (equation 28), it can be checked that $y_{\rm br}$ decreases with $\kappa_{\rm w}$, and $(1 - \alpha/y_{\rm br})^{-b}$ increases with $\kappa_{\rm w}$. From the dependence of $E_{\rm br}$, $T_{\rm br}$, $t_{\rm br}$ and $\Gamma_{\rm s,br}\beta_{\rm s,br}$ on Ψ and $y_{\rm br}$, it is not hard to understand the trend shown in Fig. 4. First, equation (30) implies that $\Gamma_{\rm s,br}\beta_{\rm s,br}$ is a strong increasing function of $\kappa_{\rm w}$. Then, equation (34) implies that $t_{\rm br}$ is a decreasing function of $\kappa_{\rm w}$. In equation (32), Ψ and $y_{\rm br}$ decrease with

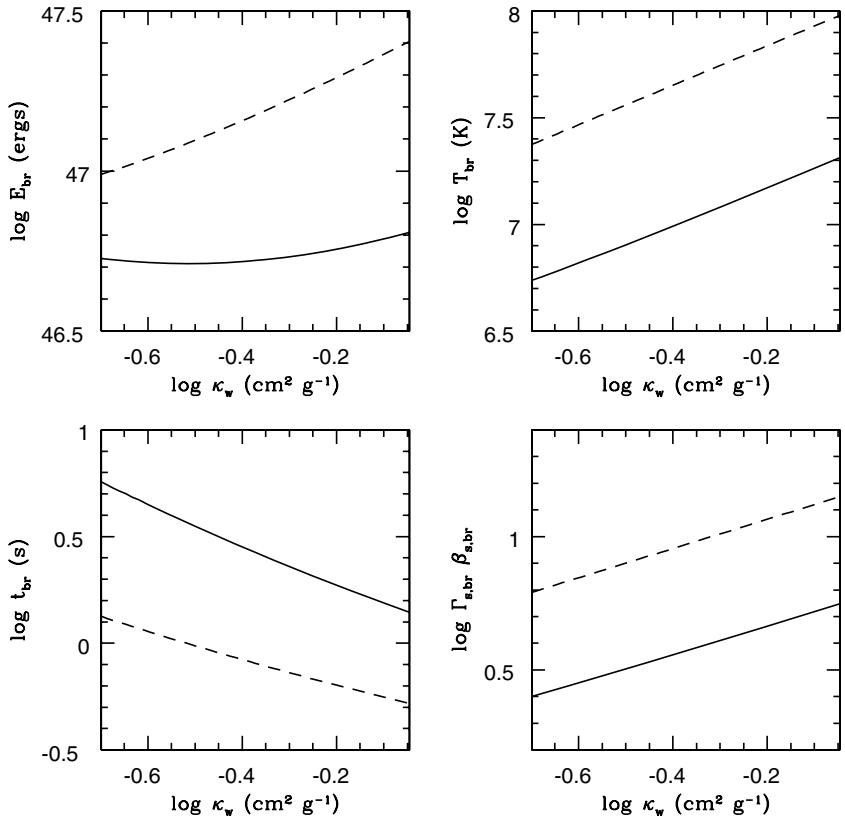

Figure 4. Characteristic quantities of shock emergence as functions of the opacity in the stellar wind. The solid line corresponds to $\varepsilon = 10^{-2}$. The dashed line corresponds to $\varepsilon = 10^{-3}$. Other parameters are $b = 5$, $E_{\rm in} = 10^{52}$ erg, $M_{\rm ej} = 10\,\rm M_\odot$ and $R_\star = 3\,\rm R_\odot$.

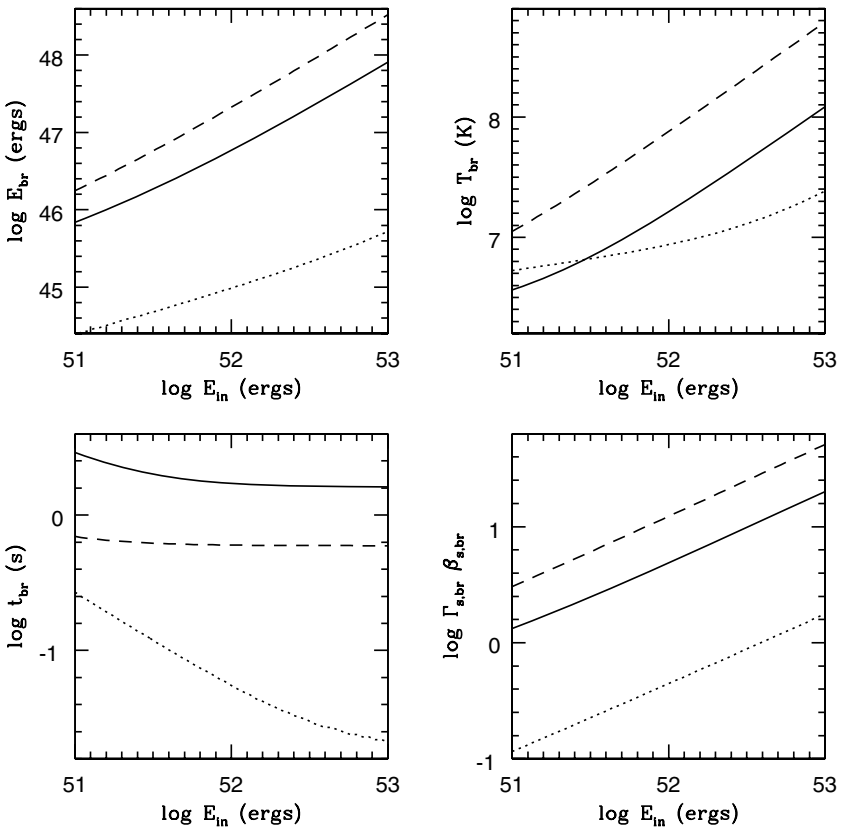

Figure 5. Characteristic quantities of shock emergence as functions of the explosion kinetic energy. The solid line corresponds to $\varepsilon = 10^{-2}$. The dashed line corresponds to $\varepsilon = 10^{-3}$. Other parameters are: $b = 5$, $\kappa_{\rm w} = 0.7$ cm^2 g^{-1}, $M_{\rm ej} = 10\,{\rm M}_\odot$, and $R_\star = 3\,{\rm R}_\odot$. The dotted line shows the solution for shock breakout from a star without a wind, with the same $M_{\rm ej}$, $R_\star$ and $\kappa_\star = 0.2$ cm^2 g^{-1}, $\zeta = 1$.

$\kappa_{\rm w}$, but $\Gamma^2_{\rm s,br}\beta^2_{\rm s,br}$ and $(1-\alpha/y_{\rm br})^{-b}$ increase with $\kappa_{\rm w}$. The overall result on $E_{\rm br}$ is that shown in the top left-hand panel of Fig. 4. Since the radius of shock breakout decreases with $\kappa_{\rm w}$, the temperature $T_{\rm br}$ must increase with $\kappa_{\rm w}$.

Fig. 5 shows the same set of characteristic quantities as functions of the explosion kinetic energy. Symbols and values of parameters are similar to those of Fig. 4 and are explained in the figure caption. To compare with the results for a star without a wind, we show with dotted lines the corresponding characteristic quantities calculated for the shock breakout from a star with the formulae in Appendix B, for the same values of $M_{\rm ej}$ and $R_\star$ and $\kappa_\star = 0.2$ cm^2 g^{-1}, $\zeta = 1$.

As the explosion energy increases from 10^{51} to 10^{53} erg, the breakout energy increases by a factor of $\approx$117 when $\varepsilon = 10^{-2}$ and $\approx$188 when $\varepsilon = 10^{-3}$. This increasing rate is much faster than that in the case of breakout from a star, in which the breakout energy increases only by a factor of $\approx$22. The increase in the temperature is also faster, which is by a factor of $\approx$33 when $\varepsilon = 10^{-2}$ and $\approx$55 when $\varepsilon = 10^{-3}$ for a star with a dense wind, and only $\approx$4.6 for a star without a wind. While for the breakout time duration, it appears that for the case of a stellar wind the time duration does not change rapidly when $E_{\rm in}$ increases, in contrast to the case of a star. This is caused by the fact that when a star is surrounded by a dense stellar wind the shock wave has more space for acceleration, and hence at the time of emergence the shock front is more relativistic (see the panel for the shock momentum), its velocity approaches the speed of light limit. As we have seen in Section 5, when the shock velocity approaches the speed of light, the breakout radius approaches $y_{\rm max}$. The distance between $y_{\rm max}$ and $y_{\rm ph}$ does not change with the explosion energy.

The momentum of the shock front varies with $E_{\rm in}$ at about the same rate for the case of a stellar wind and the case of a star.

The curvature of the curves in Fig. 5 confirms our claim at the beginning of this section that in the trans-relativistic case the characteristic quantities of shock breakout in general cannot be written as factorized scaling formulae of input parameters.

Fig. 6 shows the characteristic quantities as functions of the ejected mass. As the ejected mass $M_{\rm ej}$ increases from 1 to $20\,{\rm M}_\odot$, the breakout energy decreases by a factor of $\approx$7.8 when $\varepsilon = 10^{-2}$, and $\approx$9.1 when $\varepsilon = 10^{-3}$, faster than the case of a star for which the decreasing factor is $\approx$4.4. The temperature also drops faster. The variation in the breakout time duration is not fast in both the cases of stellar winds and stars. That is, the time duration of the shock breakout is not very sensitive to the ejected mass. The momentum of the shock front drops slightly slower than that in the case of a star.

Fig. 7 shows the characteristic quantities as functions of the core radius of the star, which, as in the case of a star (Matzner & McKee 1999), is the parameter that most dramatically affects the values of the characteristic quantities. As $R_\star$ increases from 1 to $30\,{\rm R}_\odot$, the breakout energy increases by a factor of $\approx$69 when $\varepsilon = 10^{-2}$, and $\approx$51 when $\varepsilon = 10^{-3}$. However, this factor is smaller than that in the case of star without a wind, which is $\approx$277. The temperature drops very fast, caused by the increase in the area of the surface emitting the radiation. As $R_\star$ increases from 1 to $30\,{\rm R}_\odot$, the temperature drops by a factor of $\approx$16 when $\varepsilon = 10^{-2}$, and $\approx$21 when $\varepsilon = 10^{-3}$, in contrast to the factor of $\approx$5.8 in the case of a star. The variation in the stellar radius also has a dramatic effect on the breakout time

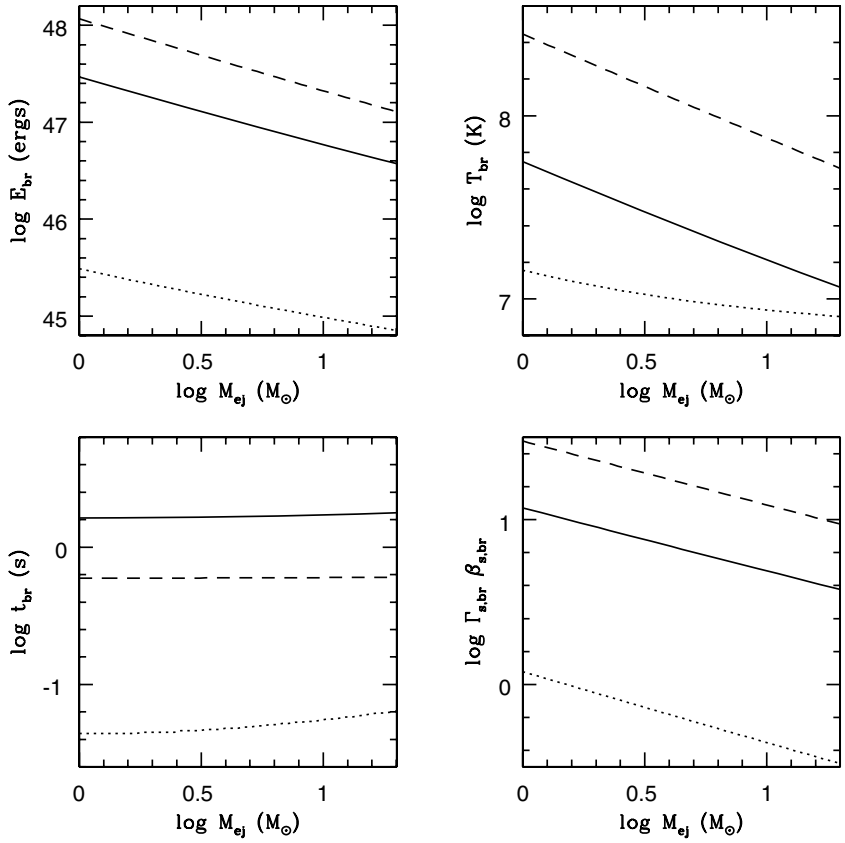

Figure 6. Characteristic quantities of shock emergence as functions of the ejected mass. The solid line corresponds to $\varepsilon = 10^{-2}$. The dashed line corresponds to $\varepsilon = 10^{-3}$. Other parameters are $b = 5$, $\kappa_{\rm w} = 0.7$ cm^2 g^{-1}, $E_{\rm in} = 10^{52}$ erg and $R_\star = 3\,{\rm R}_\odot$. The dotted line shows the solution for shock breakout from a star without a wind, with the same $E_{\rm in}$, $R_\star$ and $\kappa_\star = 0.2$ cm^2 g^{-1}, $\zeta = 1$.

duration, although the effect is less prominent than in the case of a star. The factor by which the breakout time duration increases is $\approx$43 when $\varepsilon = 10^{-2}$, and $\approx$32 when $\varepsilon = 10^{-3}$, in contrast to that of $\approx$590 in the case of a star. The momentum of the shock front drops by a factor of $\approx$4.8 when $\varepsilon = 10^{-2}$, and $\approx$4.5 when $\varepsilon = 10^{-3}$, similar to the factor of $\approx$3 in the case of a star.

Finally, in Fig. 8 we show the characteristic quantities as functions of b. The breakout energy $E_{\rm br}$ increases with b. As b increases from 1 to 10, $E_{\rm br}$ increases by a factor of $\approx$2.9 when $\varepsilon = 10^{-2}$, and $\approx$12 when $\varepsilon = 10^{-3}$. The smaller is ε, the faster does $E_{\rm br}$ increases with b. However, if b is in the range of 4–6, the change in $E_{\rm br}$ is not essential, only by a factor of $\approx$1.2–1.3. The temperature has a similar trend. When $\varepsilon = 10^{-2}$, the time duration $t_{\rm br}$ decreases with b. When $\varepsilon = 10^{-3}$, $t_{\rm br}$ decreases with b until b grows to a value $\approx$3, beyond which $t_{\rm br}$ increases but slowly. The momentum of the shock front increases with b, caused by the fact that a larger b results in a steeper density profile and an enhanced acceleration of the shock.

From Figs 4–7, and Fig. 8 at $b = 4$–6, the effects of variation in ε from 10^{-2} to 10^{-3} can be summarized as follows: the breakout energy $E_{\rm br}$ increases by a factor of 1.8–4; the temperature $T_{\rm br}$ increases by a factor of 3–5; the shock momentum $\Gamma_{\rm s,br}\beta_{\rm s,br}$ increases by a factor of 2.3–2.5; and the time duration $t_{\rm br}$ decreases by a factor of 2.3–4.3.

Figs 5–7 also show that, for a star with a dense wind, the shock breakout is more energetic than that for a star without a wind. This is not surprising since a star with a dense wind has effectively a larger radius so that the shock wave has more space and more time for acceleration. For the same set of common parameters ($E_{\rm in}$, $M_{\rm ej}$, $R_\star$, but not the opacity), for typical parameters the total energy of the radiation from shock breakout is larger by a factor of >10 if the star is surrounded by a dense wind. The momentum of the shock front is also larger by a factor of $\sim$10. The temperature does not show a universal trend because of increase in the shock breakout radius, but generally it is larger if the progenitor is surrounded by a dense wind due to the great enhancement in the breakout energy. The time duration is larger for the case of stellar winds as an obvious result of increase in the effective radius of the star.

The shock breakout occurs inside the maximum acceleration radius $R_{\rm a}$ (equation 14) in all the models presented in Figs 4–8.

In the above calculations of the breakout time duration, the light traveltime has not been taken into account. In other words, $t_{\rm br}$ is the duration measured in the SN frame. The duration observed by a remote observer, $t_{\rm br,obs}$, differs from $t_{\rm br}$ by an effect caused by the traveltime of light – which arises from the fact that an observer will see more distant annuli of the stellar disc with a time delay (Ensman & Burrows 1992). The effect of light traveltime could be extremely important when the $t_{\rm br}$ calculated by equation (34) is short, which is definitely true here since WR stars are compact. We approximate the observed time duration of the shock breakout event by

$$t_{\rm br,obs} = \sqrt{t_{\rm br}^2 + t_{\rm light}^2}, \tag{36}$$

where $t_{\rm light}$ is the light traveltime.

In the calculation of the light traveltime $t_{\rm light}$, the relativistic beaming effect must be taken into account since the shock wave in our models is relativistic (Katz 1994). In the ultrarelativistic limit, the

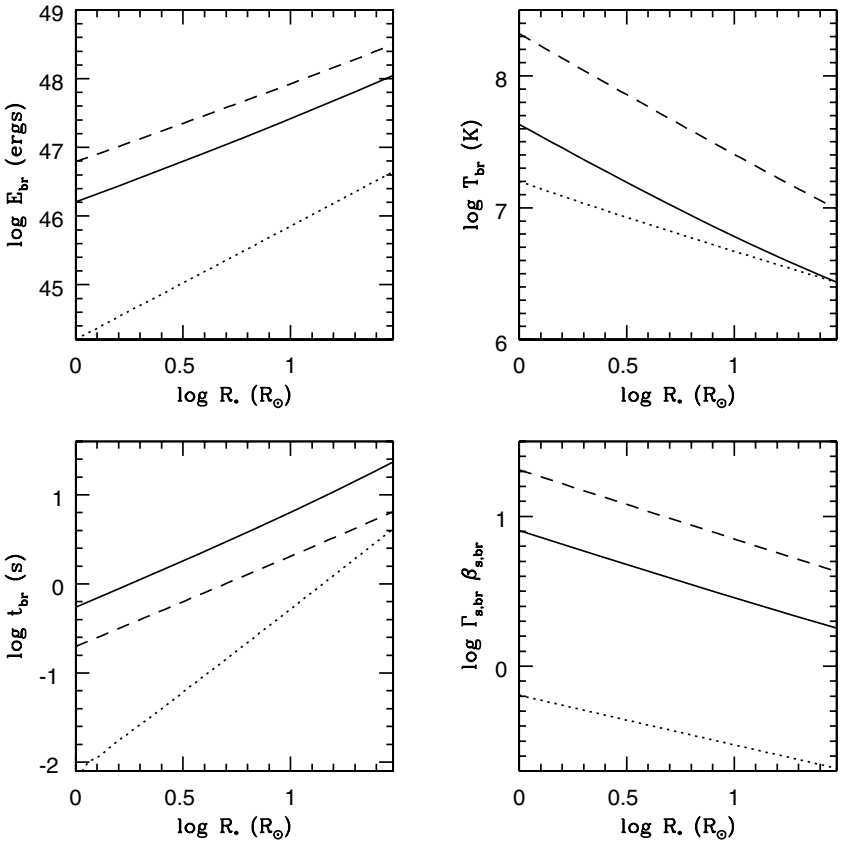

Figure 7. Characteristic quantities of shock emergence as functions of the core radius of the star. The solid line corresponds to $\varepsilon = 10^{-2}$. The dashed line corresponds to $\varepsilon = 10^{-3}$. Other parameters are: $b = 5$, $\kappa_{\rm w} = 0.7$ cm^2 g^{-1}, $E_{\rm in} = 10^{52}$ erg and $M_{\rm ej} = 10\,{\rm M}_{\odot}$. The dotted line shows the solution for shock breakout from a star without a wind, with the same $E_{\rm in}$, $M_{\rm ej}$ and $\kappa_\star = 0.2$ cm^2 g^{-1}, $\zeta = 1$.

beaming angle is $\theta \sim 1/\Gamma_{{\rm ph},X}$, where $\Gamma_{{\rm ph},X}$ is the Lorentz factor of the photosphere which can be estimated by $\Gamma_{{\rm ph},X} \approx \Gamma_{\rm s}$. In the non-relativistic limit, we should have $\theta = \pi/2$. Hence, we use an interpolation formula for θ:

$$\theta = \frac{\pi}{\pi(\Gamma_{\rm s} - 1) + 2}. \tag{37}$$

Then, the light traveltime is

$$t_{\rm light} = \frac{R_{\rm ph,X}}{c}(1 - \cos\theta). \tag{38}$$

When $\Gamma_{\rm s} \gg 1$, we have $t_{\rm light} \approx R_{\rm ph,X}/(2\Gamma_{\rm s}^2\, c)$.

For the models presented in Figs 4–8, we have calculated the light traveltime correction to the observed time duration of the shock breakout event. The results are shown in Fig. 9. It turns out that the light traveltime correction is not important. This is caused by the fact that for relativistic shock breakout the light traveltime is significantly reduced by the relativistic beaming effect.

Numerical results for a set of SN and WR star models are presented in Table 1. From these results, we find that the efficiency of converting the SN explosion energy to the shock breakout energy, defined by the ratio of the breakout energy to the explosion energy, is typically in the range of 10^{-4}–10^{-5}. This efficiency is smaller than that in the case of Type II SNe, which is typically $\sim 10^{-3}$ if the progenitor is a red supergiant, or $\sim 10^{-4}$ if the progenitor is a blue supergiant. This is again caused by the fact that WR stars have much smaller radii than red and blue supergiants.

7 APPLICATION TO GRB 060218/SN 2006aj

As stated in the Introduction, recently it has been claimed that SN shock breakout has been observed in the early X-ray emission of GRB 060218, based on the observation that a fraction ($\approx$20 per cent) of the radiation in the light curve (from 159 up to $\sim$10 000 s after the trigger of the burst) is a soft blackbody of temperature $\approx$0.17 keV (Campana et al. 2006). The total energy estimated for this blackbody component is $\approx 10^{49}$ erg in the 0.3–10 keV band, and $\approx 2 \times 10^{49}$ in bolometric (S. Campana, private communication). A reanalysis carried out by Butler (2006) revealed an even larger energy in the blackbody, which is $\approx 2 \times 10^{50}$ erg, with a duration of $\approx$300 s.

The overall constraint on the blackbody component in the early X-ray afterglow of GRB 060218 is summarized as follows: the total energy $\gtrsim 10^{49}$ erg, the temperature is in the range of 0.1–0.19 keV (i.e. 1.2–2.2 $\times$ 10^6 K) and the duration $\gtrsim$ 300 s (Butler 2006; Campana et al. 2006).

In this section, we apply the procedure developed in previous sections to calculate the characteristic quantities of the shock breakout event for SN 2006aj with the assumption that the SN was produced by the core-collapse of a WR star surrounded by a dense wind, and examine if the blackbody component in GRB 060218 can be interpreted by the shock breakout in SN 2006aj.

First, we apply the procedure to the WR stars in Fig. 1, which are among the best-studied catalogue of WR stars with model-determined stellar and photospheric radii (Hamann et al. 1995; Koesterke & Hamann 1995; Gräfener et al. 1998). We pick up only

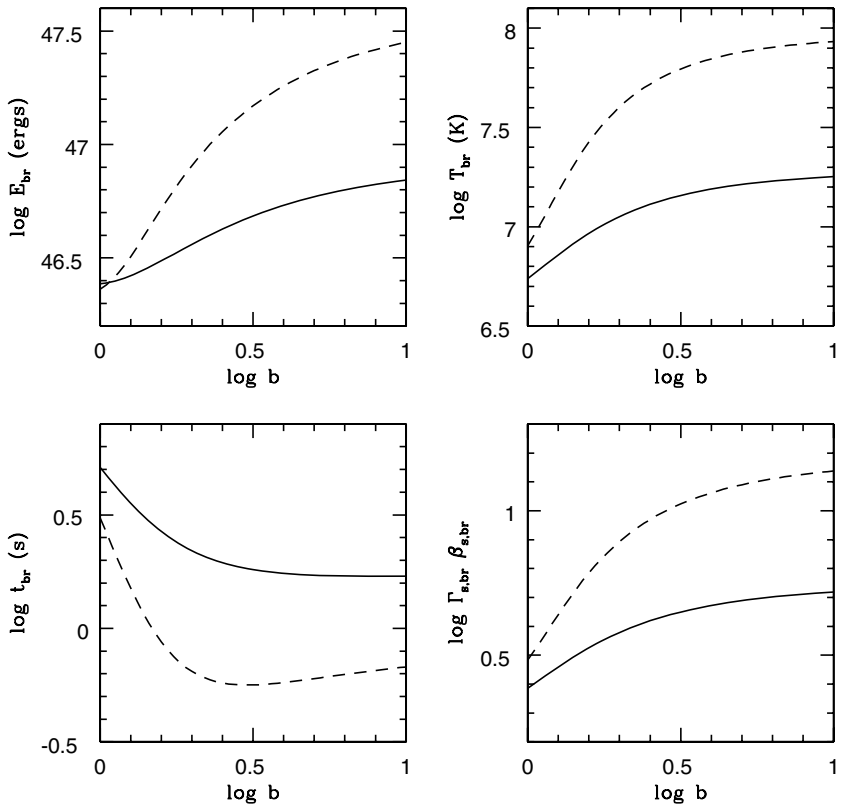

Figure 8. Characteristic quantities of shock emergence as functions of the wind parameter b. The solid line corresponds to $\varepsilon = 10^{-2}$. The dashed line corresponds to $\varepsilon = 10^{-3}$. Other parameters are: $b = 5, \kappa_{\rm w} = 0.7\ {\rm cm^2\ g^{-1}}$, $E_{\rm in} = 10^{52}$ erg, $M_{\rm ej} = 10\,{\rm M}_\odot$ and $R_\star = 3\,{\rm R}_\odot$.

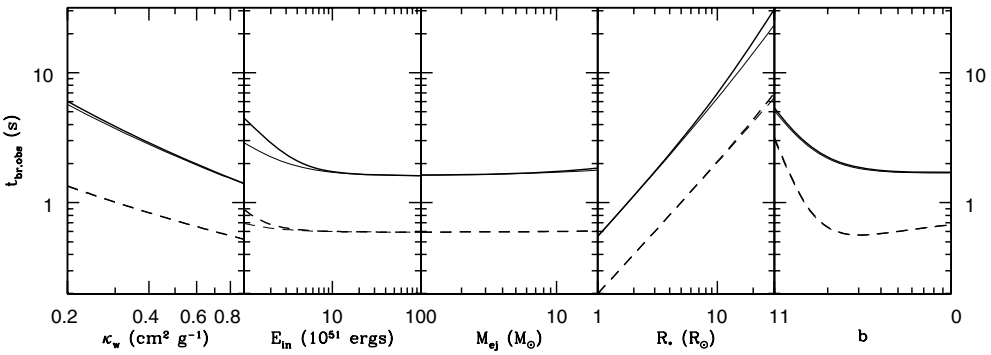

Figure 9. The observed time duration of shock breakout (defined by equation 36) for the models in Figs 4–8 (from left to right). The solid line corresponds to $\varepsilon = 10^{-2}$. The dashed line corresponds to $\varepsilon = 10^{-3}$. The thin lines are the breakout time duration $t_{\rm br}$ without the light traveltime correction (equation 34). The figure shows that in all models the light traveltime correction is not important. In some models, the thin and thick lines are even not visually distinguishable.

stars with $y_{\rm ph} = R_{\rm ph}/R_\star > 2$, since otherwise the ε given by our simplified model would be too small (Fig. 3). The sample so selected consists of total 36 stars, including 20 Galactic WCs, 10 Galactic WNs and six LMC WCs. The majority of WC stars have been included. Since these stars were modelled by the standard stellar wind model (Appendix A), we choose $b = 1$. The α parameter is then obtained from the published values of $y_{\rm ph} = R_{\rm ph}/R_\star$ in the papers cited above by equations (A2) and (A3). The value of ε is calculated with equation (3). Then, with the published values of $\dot{M}$, v_∞ and $R_\star$, the constant mean opacity $\kappa_{\rm w}$ can be calculated with equation (A5).

For the SN explosion energy and the ejected mass, we take the values obtained from modelling the spectra and the light curve of SN 2006aj: $E_{\rm in} = 2 \times 10^{51}$ erg and $M_{\rm ej} = 2\,{\rm M}_\odot$ (Mazzali et al. 2006). Then, for each star we have all of the six parameters needed for calculating the characteristic quantities of shock breakout.

Our results are shown in Fig. 10 for the breakout energy versus the breakout temperature, and in Fig. 11 for the breakout shock momentum versus the breakout time duration. Note, here the breakout time duration has included the light traveltime (equation 36), so it corresponds to the observed time duration. From Fig. 10 we see that, although the temperature is in the range of the blackbody

Table 1. Models of Type Ibc SN explosion and the predicted characteristic parameters for the shock breakout. Input parameters: $E_{\rm in}$, $M_{\rm ej}$, $R_\star$, $\kappa_{\rm w}$, ε and b. Output parameters: $y_{\rm ph,X}$, $y_{\rm br}$, $(\Gamma_{\rm s}\beta_{\rm s})_{\rm br} = \Gamma_{\rm s,br}\beta_{\rm s,br}$, $E_{\rm br}$, $T_{\rm br}$, $t_{\rm br,obs}$ and μ. Models 1–4 are normal Type Ibc SNe. Models 5–7 are hypernovae.

Model	$E_{\rm in}$[a]	$M_{\rm ej}$[b]	$R_\star$[c]	$\kappa_{\rm w}$[d]	ε[e]	b[f]	$y_{\rm ph,X}$[g]	$y_{\rm br}$[h]	$(\Gamma_{\rm s}\beta_{\rm s})_{\rm br}$[i]	$E_{\rm br}$[j]	$T_{\rm br}$[k]	$t_{\rm br,obs}$[l]	μ[m]
1	1	3	3	0.7	0.01	5	1.73	1.45	1.98	1.3	5.4	2.8	0.30
2	1	4	3	0.2	0.02	5	4.24	2.45	0.818	1.2	1.9	25	1.7
3	1.5	6	5	0.5	0.01	1	3.11	1.61	0.760	1.3	1.7	35	2.4
4	2	2	5	0.7	0.001	5	1.31	1.22	6.72	19	28	1.0	0.095
5	40	10	3	0.2	0.01	5	3.21	2.53	5.73	22	16	4.9	1.0
6	50	10	10	0.7	0.01	5	1.73	1.50	7.52	140	22	5.5	0.98
7	60	15	10	0.7	0.002	5	1.39	1.28	13.7	320	62	2.6	0.32

[a]Explosion kinetic energy in units of 10^{51} erg.
[b]Ejected mass in units of $M_\odot$.
[c]Core radius of the progenitor (the radius at the optical depth of 20) in units of $R_\odot$.
[d]Optical opacity in the wind in units of cm^2 g^{-1}.
[e]Ratio of the wind velocity at the stellar surface (where $r = R_\star$) to the terminal velocity of the wind (equation 3).
[f]Parameter specifying the profile of the wind velocity (equation 2).
[g]Radius of the X-ray photosphere in units of $R_\star$.
[h]Radius of the shock front at the time of shock breakout in units of $R_\star$.
[i]Momentum of the shock front (equation 30) at the time of shock breakout.
[j]Total energy of the radiation from the shock breakout in units of 10^{46} erg.
[k]Temperature of the radiation from the shock breakout in units of 10^6 K = 0.086 17 keV.
[l]Observed time duration of the shock breakout event in units of seconds.
[m]Observable defined by the mass-loss rate and the terminal velocity of the stellar wind through equation (9).

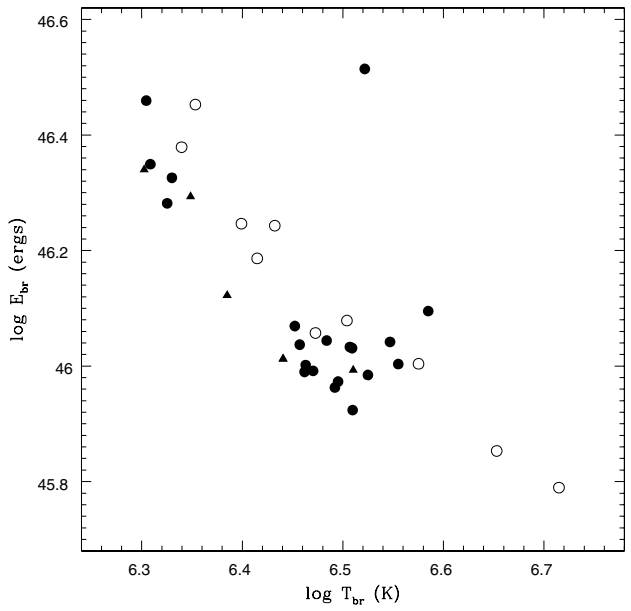

Figure 10. Energy versus temperature of shock breakout in Type Ibc SNe produced by core-collapse of a sample of WR stars with $R_{\rm ph}/R_\star > 2$.

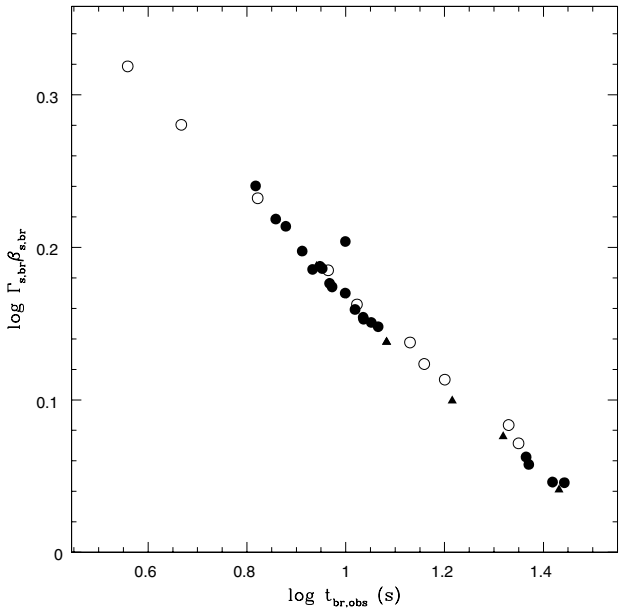

Figure 11. Shock momentum versus the observed time duration of shock breakout in Type Ibc SNe produced by core-collapse of the same sample of WRs in Fig. 10.

component in GRB 060218 for several WC stars (on the left end), the total energy of the radiation arising from the shock breakout never exceeds 10^{47} erg, i.e. always smaller than the total energy of the observed blackbody component in GRB 060218 by more than two orders of magnitude.

From Fig. 11, the time duration of the shock breakout never exceeds 100 s, also well below the observational limit on the blackbody component in GRB 060218.

Thus, it appears that none of the stars in the considered sample of WRs is able to produce a SN with shock breakout energy that is large enough to explain the blackbody component observed in the early X-ray afterglow of GRB 060218.

Of course, GRBs are rare events compared to SNe (Podsiadlowski et al. 2004), they may require progenitors that are in more extreme conditions than the WRs in our sample. To test the possibility for explaining the blackbody component in GRB 060218 with shock breakout from WR stars in a larger parameter space, we have calculated a number of models with a large range of parameters. The results are shown in Fig. 12 ($b = 5$) and Fig. 13 ($b = 1$). The explosion energy and the ejected mass are fixed at $E_{\rm in} = 2 \times 10^{51}$ erg and $M_{\rm ej} = 2\,M_\odot$, as obtained by modelling the spectra and the light curve of SN 2006aj (Mazzali et al. 2006). We allow ε to vary from 10^{-2} to 10^{-5}. For the opacity $\kappa_{\rm w}$, we choose two extreme values: 0.2 (solid lines) and 0.9 cm^2 g^{-1} (dashed lines). The

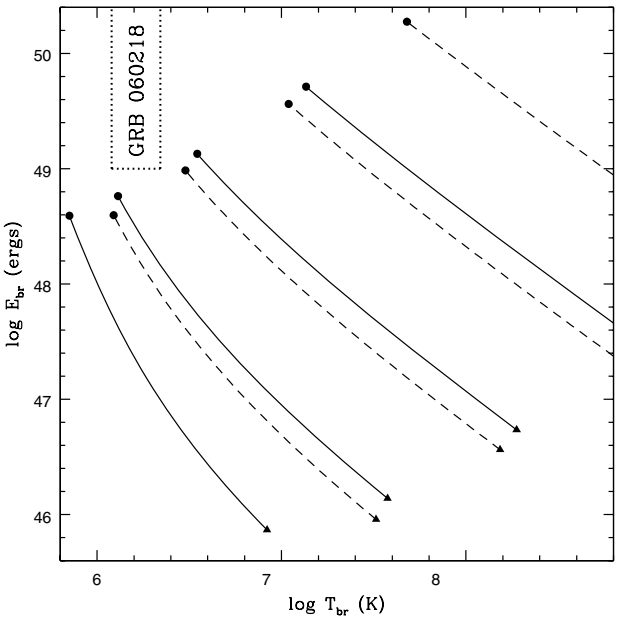

Figure 12. The breakout energy versus the breakout temperature (with $b = 5$). Solid lines correspond to $\kappa_w = 0.2\ \mathrm{cm^2\ g^{-1}}$. Dashed lines correspond to $\kappa_w = 0.9\ \mathrm{cm^2\ g^{-1}}$. Different solid lines (and different dashed lines) correspond to different values of ε: 10^{-2}, 10^{-3}, 10^{-4} and 10^{-5} (upward). Along each line, the stellar radius $R_\star$ varies from $1\,\mathrm{R_\odot}$ (the triangle) to $100\,\mathrm{R_\odot}$ (the point). The SN explosion energy $E_{in} = 2 \times 10^{51}$ erg. The ejected mass $M_{ej} = 2\,\mathrm{M_\odot}$. The region bounded by the dotted line indicates the observational constraint on the total energy and the temperature of the blackbody component in the X-ray afterglow of GRB 060218.

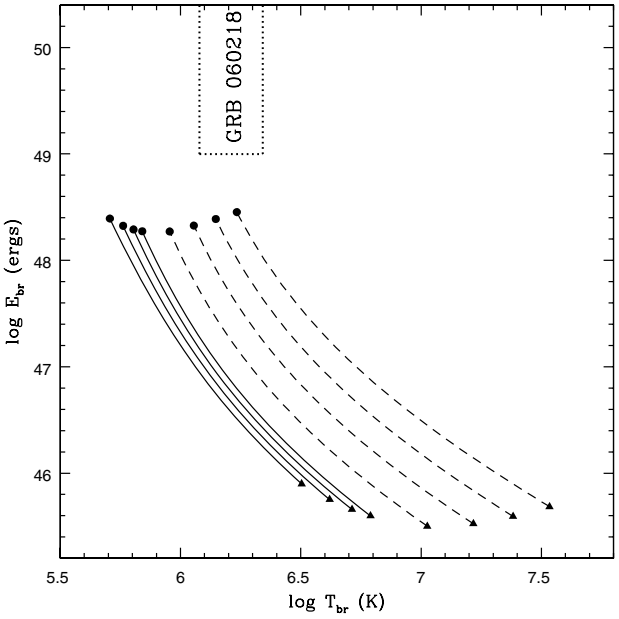

Figure 13. Same as Fig. 12 but with $b = 1$.

observational bound on the total energy and the temperature of the blackbody component in the early X-ray emission of GRB 060218 is shown in the figures by the region bounded by the dotted lines.

The radius of the star, $R_\star$, which is the parameter that the characteristic quantities of the shock breakout are most sensitive to, is allowed to vary from 1 to $100\,\mathrm{R_\odot}$, covering a space of radii that is more than enough for WR stars.

Figs 12 and 13 show that to explain the blackbody component observed in the early X-ray emission of GRB 060218, the radius of the progenitor WR star must be $\gtrsim 100\,\mathrm{R_\odot}$. It is very unlikely that there exist WR stars having so large stellar radii. Although it is possible to get $E_{br} > 10^{49}$ erg with $R_\star < 100\,\mathrm{R_\odot}$ if ε is very small and/or κ_w is very large, the corresponding T_{br} would be too high to be consistent with the temperature of the blackbody component in GRB 060218.

8 SUMMARY, CONCLUSIONS AND DISCUSSIONS

We have presented a simple model for calculating the characteristic quantities (total energy, temperature, time duration and shock momentum) for the flashes arising from shock breakout in Type Ibc SNe produced by the core-collapse of WR stars surrounded by dense stellar winds. The wind velocity is modelled by equation (2), a profile that is often adopted in the study of stellar winds. However, in contrast to the case for O-stars where the parameter b is close to unity, for WR star winds b can be much larger and is usually in the range of 4–6 (Nugis & Lamers 2002). The opacity in the wind, κ_w, is assumed to be a constant, which is a reasonable approximation for the calculation of the optical depth since the opacity varies with radius very slowly compared to the mass density of the wind (Nugis & Lamers 2002). Modelling of the opacity in the winds of WR stars indicates that κ_w is in the range of 0.3–0.9 $\mathrm{cm^2\ g^{-1}}$ (Nugis & Lamers 2002).

Our model is an extension of the existing model for calculating the characteristic quantities for SN shock breakout from a star without a wind, which is suitable for Type II SNe (Imshennik & Nadëzhin 1988, 1989; Matzner & McKee 1999; Tan et al. 2001). Due to the compactness of WR stars, the shock momentum is expected to be trans-relativistic at the time of breakout. Thus, we have followed Blandford & McKee (1976) and Tan et al. (2001) to take into account the relativistic effects.

Because of the large optical depth in the wind, the SN shock breakout occurs in the wind region rather than in the interior of the star. This is equivalent to say that the presence of a dense stellar wind effectively increases the radius of the star. As a result, the shock has more space and more time for acceleration, and the shock breakout appears to be more energetic than in the case for the same star but the effect of the stellar winds is not taken into account (see e.g. Blinnikov et al. 2002).

The formulae for determining the radius where the shock breakout occurs and that for computing the characteristic quantities for the radiation arising from the shock breakout are collected in Section 5. They include equations (28), determining the breakout radius; (30), evaluating the momentum of the shock; (32), (33) and (34), calculating the energy, temperature and the time duration of the radiation from shock breakout. Although exact and analytic solutions are impossible because of the trans-relativistic nature of the problem, all the equations are algebraic and a simple numerical program is able to calculate all the characteristic quantities. The model contains six input parameters: the explosion kinetic energy (E_{in}), the ejected mass (M_{ej}), the core radius of the star ($R_\star$, the radius where the optical depth $\tau_w = 20$), the opacity in the wind (κ_w), the parameter b specifying the wind velocity profile and the ratio of the wind velocity at the stellar surface (where $r = R_\star$) to the terminal velocity of the wind (ε).

Our numerical results are summarized in Figs 4–8 and Table 1. Figs 4–8 illustrate how the characteristic quantities vary with the input parameters. As in the case of shock breakout from a star without

a wind, the core radius of the star is the most important parameter affecting the results. That is, the characteristic quantities are most sensitive to the variation in the stellar radius. This feature leads to the possibility for distinguishing the progenitors of SNe by observing the flashes from the shock breakout (Calzavara & Matzner 2004). In addition, in the case of dense stellar winds, the results are more sensitive to the variation in the SN explosion kinetic energy. For example, roughly speaking, $E_{\rm br} \propto E_{\rm in}$ when the star has a dense wind, in contrast to $E_{\rm br} \propto E_{\rm in}^{0.6}$ in the case of a star without a wind. Overall, the shock breakout from a star with a dense wind is more energetic than that from a star without a wind. For a star of the same radius, and for the same explosion kinetic energy and ejected mass, the total energy released by the shock breakout is larger by a factor of >10 if the star is surrounded by a thick wind. The time duration is also larger, and the shock momentum at the time of breakout is more relativistic.

For explosion energy $E_{\rm in} = 10^{51}$ erg, ejected mass $M_{\rm ej} = 3\,{\rm M}_\odot$, and stellar radius $R_\star = 3\,{\rm R}_\odot$ (typical values for normal Type Ibc SNe), we get breakout energy $E_{\rm br} \approx 1.3 \times 10^{46}$ erg, temperature $T_{\rm br} \approx 5.4 \times 10^6$ K $\approx$0.46 keV and observed time duration $t_{\rm br,obs} \approx$ 2.8 s if other parameters take fiducial values ($\kappa = 0.7$ cm^2 g^{-1}, $b = 5$ and $\varepsilon = 0.01$). For $E_{\rm in} = 5 \times 10^{52}$ erg, $M_{\rm ej} = 10\,{\rm M}_\odot$ and $R_\star = 10\,{\rm R}_\odot$ (typical values for hypernovae), we get $E_{\rm br} \approx 1.4 \times 10^{48}$ erg, $T_{\rm br} \approx 2.2 \times 10^7$ K $\approx$1.9 keV and $t_{\rm br,obs} \approx 5.5$ s. More numerical results are shown in Table 1.

We have applied our model to GRB 060218/SN 2006aj, in which a soft blackbody component has been observed in the early X-ray emission of the GRB and has been interpreted as evidence for the SN shock breakout (Campana et al. 2006). We take the values of the SN explosion energy and the ejected mass obtained from modelling the spectra and the light curve of the SN (Mazzali et al. 2006). We find that, the energy released by the SN shock breakout in a thick wind of a WR progenitor star is generally too small to explain the blackbody radiation in GRB 060218. To obtain the breakout energy and the temperature that are consistent with the observational constraint, the core radius of the progenitor WR star has to be $>100\,{\rm R}_\odot$, which is too large for a WR star. Thus, we conclude that the blackbody component in the X-ray afterglow of GRB 060218 cannot be interpreted by the shock breakout in the underlying SN. Instead, it must originate from other processes which might be related to the GRB outflow (see e.g. Fan, Piran & Xu 2006). This conclusion is in agreement with the analysis by Ghisellini, Ghirlanda & Tavecchio (2006).

One may argue that GRB-connected SNe should be highly aspherical so that our spherical model might have underestimated the energy of the shock breakout. The effect of explosion asymmetry can be estimated as follows. Assume that the explosion produces a shock wave in a solid angle $\Omega \equiv 4\pi\omega < 4\pi$ with a kinetic explosion energy $E_{\rm in}$, which ejects a mass $M_{\rm ej}$ from the progenitor. The shock wave is symmetric in the azimuthal direction and does not expand to the outside of Ω. The motion of the shock wave would then be the same as that of a spherical shock wave ($\omega = 1$) with a kinetic explosion energy $\omega^{-1}E_{\rm in}$ and an ejected mass $\omega^{-1}M_{\rm ej}$, assuming that the progenitor is spherically symmetric. Then, by equation (30), $p \propto E_{\rm in}^{1/2} M_{\rm ej}^{-0.313} \omega^{-0.187} = (\omega^{-0.374} E_{\rm in})^{1/2} M_{\rm ej}^{-0.313}$. That is, the motion of the asymmetric shock wave can be calculated by equation (30) but with $E_{\rm in}$ replaced by a larger $E'_{\rm in} = \omega^{-0.374} E_{\rm in}$. Then, by Fig. 5, the temperature $T_{\rm br}$, the shock momentum $\Gamma_{\rm s,br}\beta_{\rm s,br}$ and the isotropic equivalent energy $E_{\rm br}$ of the asymmetric shock breakout are larger than those in a spherical explosion with the same $E_{\rm in}$ and $M_{\rm ej}$. However, the time duration $t_{\rm br}$ is not sensitive to ω.

Indeed, aspherical explosion has been claimed to be observed in the luminous Type Ic SN 2003jd, in which the double-lined profiles in the nebular lines of neutral oxygen and magnesium revealed in later time observations by Subaru and Keck are explained as results of observing an aspherical SNe along a direction almost perpendicular to the axis of the explosion (Mazzali et al. 2005). However, for SN 2006aj, there is no evidence for aspherical explosion. Observation on the radio afterglow and modelling of it indicates that the outflow associated with GRB 060218 is mildly relativistic so should be more or less spherical (Fan et al. 2006; Soderberg et al. 2006; see also Li 2006).

We should also remark that whether the progenitors of GRBs are surrounded by dense winds is still an open question. Although a wind-type density profile is naturally expected for the environment surrounding a GRB as its progenitor is broadly thought to be a massive star, observations on the GRB afterglows have revealed that most of the afterglow data are consistent with a constant density external medium and only a handful of bursts can be well modelled by the wind model (Berger et al. 2003; Zhang & Mészáros 2004; Panaitescu 2005; Fryer, Rockefeller & Young 2006 and references therein). For the case of GRB 060218, modelling of its radio afterglow also does not favour a dense circum-burst wind profile (Fan et al. 2006; Soderberg et al. 2006).

A theoretical argument against strong winds surrounding GRB progenitors comes from the consideration of angular momentum (Yoon & Langer 2005; Woosley & Heger 2006a and references therein). For a black hole formed from the core-collapse of a massive star to have a disc rotating around it and to launch a relativistic jet, the progenitor star must rotate rapidly with the specific angular momentum in the core $j \gtrsim 3 \times 10^{16}$ cm^2 s^{-1} (MacFadyen & Woosley 1999). To satisfy this requirement, the progenitor star should not have had a phase with an intense stellar wind since a dense wind is very effective in removing angular momentum. Given the fact that the mass-loss rate of a star sensitively depends on its metallicity (Vink & de Koter 2005) and the observations that GRBs prefer to occur in galaxies with low metallicity (Fynbo et al. 2003; Hjorth et al. 2003a; Le Floc'h et al. 2003; Sollerman et al. 2005; Fruchter et al. 2006; Stanek et al. 2006), it is reasonable to expect that the progenitors of GRBs should not have dense stellar winds surrounding them. Even in this situation, however, the radius of the massive progenitor star is also very unlikely to be large enough ($>100\,{\rm R}_\odot$) to explain the blackbody component in GRB 060218 since its progenitor star has only a mass $\sim$20 M$_\odot$ as obtained by modelling the SN light curve and spectra (Mazzali et al. 2006). In addition, if the progenitor does not have a thick wind, then in calculating the results for the shock breakout one should use the formulae in Appendix B for a star without a wind. However, in Section 6 we have seen that the formulae for a star without a wind lead to smaller total energy in the radiation from the shock breakout than the formulae for a star with a dense wind.

In spite of the disappointing result on GRB 060218/SN 2006aj, our model is expected to have important applications to Type Ibc SNe since whose progenitors are broadly believed to be WR stars. In addition, some Type II SNe appear also to be related to progenitor stars with intensive stellar winds, e.g. Type IIn SNe (also called IIdw) (Hamuy 2004). Observations on the transient events from SN shock breakout will be the most powerful approach for diagnosing the progenitors of SNe. For this goal, we would like to mention *LOBSTER*, an upcoming space observatory dedicated to detect soft X-ray flashes from shock breakout in SNe (Calzavara & Matzner 2004).

ACKNOWLEDGMENTS

The author thanks S. Campana for useful communications and sharing data, and B. Paczyński for many inspiring discussions on GRBs, SNe and shock breakout. He also thanks an anonymous referee for a very helpful report which led to significant improvements to the paper.

REFERENCES

Akhiezer A. I., Berestetskii V. B., 1965, Quantum Electrodynamics. Wiley, New York
Berger E., Kulkarni S. R., Frail D. A., 2001, ApJ, 560, 652
Berger E., Soderberg A. M., Frail D. A., Kulkarni S. R., 2003, ApJ, 587, L5
Blandford R. D., McKee C. F., 1976, Phys. Fluids, 19, 1130
Blinnikov S. I., Eastman R., Bartunov O. S., Popolitov V. A., Woosley S. E., 1998, ApJ, 496, 454
Blinnikov S., Lundqvist P., Bartunov O., Nomoto K., Iwamoto K., 2000, ApJ, 532, 1132
Blinnikov S. I., Nadyozhin D. K., Woosley S. E., Sorokina E. I., 2002, in Hillebrandt W., Müller E., eds, Nuclear Astrophysics. Max-Planck-Institut für Astrophysik, Garching, p. 144
Bloom J. S., Djorgovski S. G., Kulkarni S. R., Frail D. A., 1998, ApJ, 507, L25
Bloom J. S. et al., 1999, ApJ, 518, L1
Butler N. R., 2006, ApJ, in press (astro-ph/0604083)
Calzavara A. J., Matzner C. D., 2004, MNRAS, 351, 694
Campana S. et al., 2006, Nat, 442, 1008
Chen H.-W., Prochaska J. X., Bloom J. S., 2006, in Holt S. S., Gehrels N., Nousek J. A., eds, Sixteenth Maryland Astrophysics Conference. Gamma-Ray Bursts in the Swift Era. Am. Inst. Phys., New York, p. 534
Chevalier R. A., Klein R. I., 1979, ApJ, 234, 597
Christensen L., Hjorth J., Gorosabel J., 2004, A&A, 425, 913
Cobb B. E., Bailyn C. D., van Dokkum P. G., Natarajan P., 2006, ApJ, 645, L113
Colgate S. A., 1968, Can. J. Phys., 46, S476
Costa E. et al., 1997, Nat, 387, 783
Della Valle M., 2006, in Holt S. S., Gehrels N., Nousek J. A., eds, Sixteenth Maryland Astrophysics Conference, Gamma-Ray Bursts in the Swift Era. Am. Inst. Phys., New York, p. 367
Ensman L., Burrows A., 1992, ApJ, 393, 742
Fan Y., Piran T., Xu D., 2006, JCAP, 09, 013
Filippenko A. V., 2004, in Humphreys R., Stanek K., eds, The Fate of the Most Massive Stars. Astron. Soc. Pac., San Francisco, p. 34
Frail D. A., Kulkarni S. R., Nicastro S. R., Feroci M., Taylor G. B., 1997, Nat, 389, 261
Frail D. A. et al., 2002, ApJ, 565, 829
Fruchter A. S. et al., 1999a, ApJ, 516, 683
Fruchter A. S. et al., 1999b, ApJ, 519, L13
Fruchter A. S. et al., 2006, Nat, 441, 463
Fryer C. L., Rockefeller G., Young P. A., 2006, ApJ, 647, 1269
Fynbo J. P. U. et al., 2003, A&A, 406, L63
Galama T. J. et al., 1998, Nat, 395, 670
Ghisellini G., Ghirlanda G., Tavecchio F., 2006, MNRAS, in press (doi:10.1111/j.1745-3933.2006.00270.x) (astro-ph/0608555)
Gnatyk B. I., 1985, Sov. Astron. Lett., 11, 331
Gräfener G., Hamann W.-R., 2005, A&A, 432, 633
Gräfener G., Hamann W.-R., Hillier D. J., Koesterke L., 1998, A&A, 329, 190
Hamann W.-R., Koesterke L., Wessolowski, 1995, A&A, 299, 151
Hammer F., Flores H., Schaerer D., Dessauges-Zavadsky M., Le Floc'h E., Puech M., 2006, A&A, 454, 103
Hamuy M., 2004, in Fryer C. L., ed., Stellar Collapse. Kluwer, Dordrecht, p. 39
Hjorth J. et al., 2003a, ApJ, 597, 699
Hjorth J. et al., 2003b, Nat, 423, 847
Ignace R., Oskinova L. M., Foullon C., 2000, MNRAS, 318, 214
Imshennik V. S., Nadëzhin D. K., 1988, Sov. Astron. Lett., 14, 449
Imshennik V. S., Nadëzhin D. K., 1989, Astrophys. Space Phys. Rev., 8, 1
Iwamoto K. et al., 1998, Nat, 395, 672
Katz J. I., 1994, ApJ, 422, 248
Klein R. I., Chevalier R. A., 1978, ApJ, 223, L109
Klose S. et al., 2004, AJ, 128, 1942
Koesterke L., Hamann W.-R., 1995, A&A, 299, 503
Krolik J. H., Kallman T. R., 1984, ApJ, 286, 366
Langer N., 1989, A&A, 210, 93
Le Floc'h E. et al., 2003, A&A, 400, 499
Lépine S., Moffat A. F. J., 1999, ApJ, 514, 909
Li L.-X., 2006, MNRAS, 372, 1357
Liang E., Zhang B., Dai Z. G., 2006, preprint (astro-ph/0605200)
MacFadyen A. I., Woosley S. E., 1999, ApJ, 524, 262
Malesani D. et al., 2004, ApJ, 609, L5
Masetti N., Palazzi E., Pian E., Patat F., 2006, GCN, 4803
Matzner C. D., McKee C. F., 1999, ApJ, 510, 379
Mazzali P. A. et al., 2005, Sci, 308, 1284
Mazzali P. A., Deng J., Nomoto K., Pian E., Tominaga N., Tanaka M., Maeda K., 2006, Nat, 442, 1018
Mirabal N. et al., 2003, ApJ, 595, 935
Mirabal N., Halpern J. P., An D., Thorstensen J. R., Terndrup D. M., 2006, ApJ, 643, L99
Modjaz M. et al., 2006, ApJ, 645, L21
Nugis T., Lamers H. J. G. L. M., 2000, A&A, 360, 227
Nugis T., Lamers H. J. G. L. M., 2002, A&A, 389, 162
Paczyński B., 1998a, ApJ, 494, L45
Paczyński B., 1998b, in Meegan C. A., Preece R. D., Koshut T. M., eds, 4th Huntsville Symp., Gamma-Ray Bursts. Am. Inst. Phys., New York, p. 783
Panaitescu A., 2005, MNRAS, 363, 1409
Pian E. et al., 2006, Nat, 442, 1011
Piran T., 2004, Rev. Mod. Phys., 76, 1143
Podsiadlowski Ph., Mazzali P. A., Nomoto K., Lazzati D., Cappellaro E., 2004, ApJ, 607, L17
Robert C., 1994, Ap&SS, 221, 137
Sazonov S. Yu., Lutovinov A. A., Sunyaev R. A., 2004, Nat, 430, 646
Schaefer B. E. et al., 2003, ApJ, 588, 387
Schaerer D., 1996, A&A, 309, 129
Schaerer D., Maeder A., 1992, A&A, 263, 129
Schmutz W., 1997, A&A, 321, 268
Smartt S. J., Vreeswijk P. M., Ramirez-Ruiz E., Gilmore G. F., Meikle W. P. S., Ferguson A. M. N., Knapen J. H., 2002, ApJ, 572, L147
Soderberg A. M. et al., 2006, Nat, 442, 1014
Sollerman J., Östlin G., Fynbo J. P. U., Hjorth J., Fruchter A., Pedersen K., 2005, New. Astron., 11, 103
Sollerman J. et al., 2006, A&A, 454, 503
Stanek K. Z. et al., 2003, ApJ, 591, L17
Stanek K. Z. et al., 2006, ApJ, submitted (astro-ph/0604113)
Tan J. C., Matzner C. D., McKee C. F., 2001, ApJ, 551, 946
van Paradijs J. et al., 1997, Nat, 386, 686
Vink J. S., de Koter A., 2005, A&A, 442, 587
Woosley S. E., Bloom J. S., 2006, ARA&A, 44, 507
Woosley S. E., Heger A., 2006a, ApJ, 637, 914
Woosley S. E., Heger A., 2006b, in Holt S. S., Gehrels N., Nousek J. A., eds, Sixteenth Maryland Astrophysics Conference, Gamma-Ray Bursts in the Swift Era. Am. Inst. Phys., New York, p. 398
Woosley S. E., Heger A., Weaver T. A., 2002, Rev. Mod. Phys., 74, 1015
Yoon S.-C., Langer N., 2005, A&A, 443, 643
Zeh A., Klose S., Hartmann D. H., 2004, ApJ, 609, 952
Zhang B., Mészáros P., 2004, Int. J. Mod. Phys. A, 19, 2385

APPENDIX A: OPTICAL DEPTH IN A WIND IN THE STANDARD MODEL

In the standard model of stellar winds the parameter b in equation (2) is assumed to be unity. Then, the integral in equation (4) gives

$$\tau_{\rm w} = \tau_0 \ln\left(1 - \frac{\alpha}{y}\right)^{-1}, \tag{A1}$$

where

$$\tau_0 \equiv \frac{A}{\alpha R_\star} = \frac{20}{\ln(1-\alpha)^{-1}}. \tag{A2}$$

The ratio of the photospheric radius (at $\tau_{\rm w} = 2/3$) to the stellar core radius (at $\tau_{\rm w} = 20$) is

$$y_{\rm ph} = \frac{\alpha}{1 - \exp[-2/(3\tau_0)]}, \tag{A3}$$

which approaches 1 as $\alpha \to 1$, and 30 as $\alpha \to 0$.

The X-ray photospheric radius is

$$y_{\rm ph,X} = \frac{\alpha}{1 - \exp[-2/(3\iota\tau_0)]}. \tag{A4}$$

The corresponding mass function Ψ (equation 16), when $\dot{M}$ and v_∞ are eliminated (by using equation A2), is

$$\Psi = \frac{80\pi\alpha R_\star^2}{\kappa_{\rm w} \ln(1-\alpha)^{-1}}. \tag{A5}$$

The parameter $\xi = |\partial \ln \tau_{\rm X}/\partial \ln r|^{-1}$ (Section 4) is

$$\xi = \frac{y}{\alpha}\left(1 - \frac{\alpha}{y}\right) \ln\left(1 - \frac{\alpha}{y}\right)^{-1}, \tag{A6}$$

which approaches unity as $y \to \infty$, and approaches zero as $y \to \alpha$.

The maximum radius, where the shock breakout occurs (see Section 5), is given by

$$y_{\rm max} = \frac{\alpha}{1 - \exp(-1/\iota\tau_0)}. \tag{A7}$$

APPENDIX B: SHOCK BREAKOUT FROM A STAR WITHOUT A WIND

The mass density in an outer layer of a star is described by a power law (see e.g. Matzner & McKee 1999)

$$\rho = \rho_1 x^n, \tag{B1}$$

where $x \equiv 1 - r/R_\star$, n is related to the polytropic index $\hat{\gamma}$ by $\hat{\gamma} = 1 + 1/n$. When $\hat{\gamma} = 4/3$, we have $n = 3$.

The optical depth in the star is

$$\tau_\star = \tau_0 x^{n+1}, \quad \tau_0 \equiv \frac{\kappa_\star \rho_1 R_\star}{n+1}, \tag{B2}$$

where $\kappa_\star$ is the opacity.

Near the stellar surface we have $r \approx R_\star$, so the shock accelerates according to equation (13) with $m \approx M_{\rm ej}$ and $r \approx R_\star$ (Tan et al. 2001).

The geometric thickness of the shock front is

$$\Delta r_{\rm s} \approx \frac{\tau_{\rm s}}{\Gamma_{\rm s}^2 \kappa_\star \rho} = \xi \frac{\tau_{\rm s}}{\tau_\star} \frac{R_\star x}{\Gamma_{\rm s}^2}, \tag{B3}$$

where $\xi = 1/(n+1)$, $\tau_{\rm s} = c/v_{\rm s}$.

The shock breakout occurs at a radius where $\tau_\star = \tau_{\rm s}$. The minimum value of $x_{\rm br}$, which occurs when $v_{\rm s} \to c$, is

$$x_{\rm min} = \tau_0^{-1/(n+1)} \tag{B4}$$

corresponding to the maximum breakout radius $r_{\rm max} = R_\star(1 - x_{\rm min})$.

The pressure of the gas behind the shock front, measured in the frame of the shocked gas, is still given by equation (21), from which the temperature of the shock emergence can be calculated.

The total energy of radiation in the shock emergence, measured in the rest frame, is

$$E_{\rm br} \approx 4\pi\xi F_\gamma^2 F_p \rho R_\star^3 (\Gamma_{\rm s} v_{\rm s})^2 x\Big|_{r=R_{\rm br}}. \tag{B5}$$

The time duration of the shock breakout is

$$t_{\rm br} \approx \frac{R_\star x_{\rm br}}{v_{\rm s,br}}. \tag{B6}$$

The input parameters include $E_{\rm in}$, $M_{\rm ej}$, $R_\star$, $\kappa_\star$ and $\zeta \equiv \rho_1/\rho_\star$, where $\rho_\star \equiv M_{\rm ej}/R_\star^3$.

APPENDIX C: A CORRELATION IN WR STAR PARAMETERS

From the parameters of the 92 Galactic and LMC WR stars presented in Fig. 1, a correlation between $\Psi = \dot{M} R_\star / v_\infty$ (equation 16) and $R_{\rm ph}$ can be derived.

In Fig. C1, we plot $\log \Psi$ against $\log R_{\rm ph}$ for the 92 WRs. Clearly, there is a strong correlation between Ψ and $R_{\rm ph}$. The relation is best fitted by

$$\log \Psi = -10.87 + 2.36 \log R_{\rm ph} \tag{C1}$$

for all stars, and

$$\log \Psi = -10.42 + 1.77 \log R_{\rm ph} \tag{C2}$$

for WC stars only, where Ψ is in unit of $\rm M_\odot$ and $R_{\rm ph}$ is in unit of $\rm R_\odot$.

To the knowledge of the author, the relation does not exist in the literature so is presented here, although it is irrelevant to the subject of the paper.

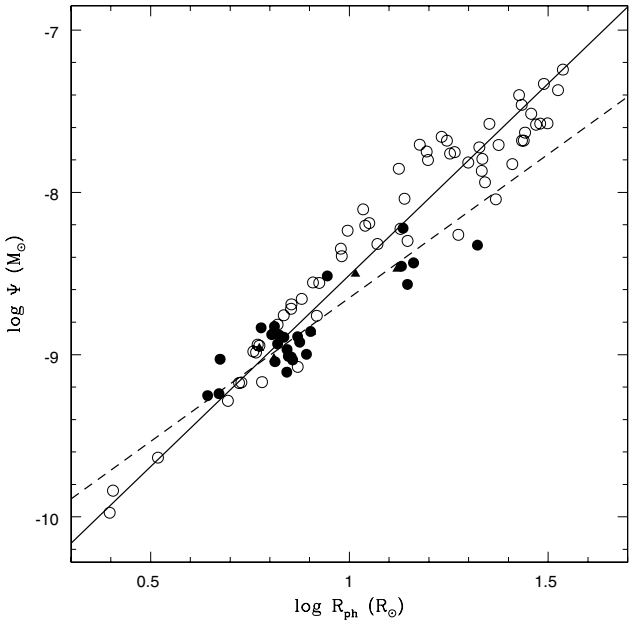

Figure C1. The mass function Ψ (defined by equation 16) against the photospheric radius for the sample of WRs in Fig. 1. Clearly, there is a strong correlation between Ψ and $R_{\rm ph}$. The solid straight line is the best fit to all the data by equation (C1). The dashed straight line is the best fit to the WC stars (filled symbols) by equation (C2).

This paper has been typeset from a TEX/LATEX file prepared by the author.